

1

2

3 **Transmigration of *Trypanosoma cruzi* trypomastigotes through 3D**
4 **cultures resembling a physiological environment**

5

6 Matías Exequiel Rodríguez¹, Mariana Rizzi¹, Lucas D. Caeiro¹, Yamil E.
7 Masip¹, Alina Perrone², Daniel O. Sánchez¹, Jacqueline Búa², Valeria
8 Tekiel^{1*}

9

10 ¹Instituto de Investigaciones Biotecnológicas “Dr. R. Ugalde” (IIBIO)
11 Universidad Nacional de San Martín (UNSAM) - CONICET, San Martín,
12 Provincia de Buenos Aires, Argentina.

13 ²Instituto Nacional de Parasitología ‘Dr Mario Fatala Chaben’, ANLIS CG
14 Malbrán. Buenos Aires, Argentina.

15

16 * Corresponding author

17 E-mail: valet@iib.unsam.edu.ar; vtekiel@gmail.com

18

19

20 **Abstract**

21 Chagas' disease, caused by the kinetoplastid parasite *Trypanosoma cruzi*,
22 presents a variety of chronic clinical manifestations whose determinants are still
23 unknown but probably influenced by the host-parasite interplay established
24 during the first stages of the infection, when bloodstream circulating
25 trypomastigotes disseminate to different organs and tissues. After leaving the
26 blood, trypomastigotes must migrate through tissues to invade cells and
27 establish a chronic infection. How this process occurs remains unexplored.
28 Three-dimensional (3D) cultures are physiologically relevant because mimic the
29 microarchitecture of tissues and provide an environment similar to the
30 encountered in natural infections. In this work, we combined the 3D culture
31 technology with host-pathogen interaction, by studying transmigration of
32 trypomastigotes into 3D spheroids. *T. cruzi* strains with similar infection
33 dynamics in 2D monolayer cultures but with different *in vivo* behavior (CL
34 Brener, virulent; SylvioX10 no virulent) presented different infection rates in
35 spheroids (CL Brener ~40%, SylvioX10 <10%). Confocal microscopy images
36 evidenced that trypomastigotes from CL Brener and other highly virulent strains
37 presented a great ability to transmigrate inside 3D spheroids: as soon as 4 hours
38 post infection parasites were found at 50 μ m in depth inside the spheroids. CL
39 Brener trypomastigotes were evenly distributed and systematically observed in
40 the space between cells, suggesting a paracellular route of transmigration to
41 deepen into the spheroids. On the other hand, poor virulent strains presented a
42 weak migratory capacity and remained in the external layers of spheroids
43 (<10 μ m) with a patch-like distribution pattern. The invasiveness -understood as
44 the ability to transmigrate deep into spheroids- was not a transferable feature

45 between strains, neither by soluble or secreted factors nor by co-cultivation of
46 trypomastigotes from invasive and non-invasive strains. We also studied the
47 transmigration of recent *T. cruzi* isolates from children that were born
48 congenitally infected, which showed a high migrant phenotype while an isolate
49 from an infected mother (that never transmitted the infection to any of her 3
50 children) was significantly less migratory. Altogether, our results demonstrate
51 that in a 3D microenvironment each strain presents a characteristic migration
52 pattern and distribution of parasites in the spheroids that can be associated to
53 their *in vivo* behavior. Certainly, the findings presented here could not have been
54 studied with traditional 2D monolayer cultures.

55

56 **Author Summary**

57 *Trypanosoma cruzi* is the protozoan parasite that causes Chagas' disease, also
58 known as American trypanosomiasis. Experimental models of the infection
59 evidence that different strains of the parasite present different virulence in the
60 host, which cannot be always reproduced in 2D monolayer cultures. Three
61 dimensional (3D) cultures can be useful models to study complex host-parasite
62 interactions because they mimic *in vitro* the microarchitecture of tissues and
63 provide an environment similar to the encountered in natural infections. In
64 particular, spheroids are small 3D aggregates of cells that interact with each
65 other and with the extracellular matrix that they secrete resembling the original
66 microenvironment both functionally and structurally. Spheroids have rarely been
67 employed to explore infectious diseases and host-parasite interactions. In this
68 work we studied how bloodstream trypomastigotes transmigrate through 3D

69 spheroids mimicking the picture encountered by parasites in tissues soon after
70 leaving circulation. We showed that the behavior of *T. cruzi* trypomastigotes in
71 3D cultures reflects their *in vivo* virulence: virulent strains transmigrate deeply
72 into spheroids while non-virulent strains remain in the external layers of
73 spheroids. Besides, this work demonstrates the usefulness of 3D cultures as an
74 accurate *in vitro* model for the study of host-pathogen interactions that could not
75 be addressed with conventional monolayer cultures.

76

77 **Introduction**

78 The protozoan parasite *Trypanosoma cruzi* is the etiological agent of Chagas
79 disease, which currently affects about 8 million people. Chagas' disease is an
80 endemic illness in Latin America that has spread worldwide in the past years.
81 The infection usually develops as a chronic cardiac, digestive or neurologic
82 pathology. The reason why symptoms appear 10 or more years after the initial
83 infection, and only in ~40% of individuals, remains unsolved, but both host and
84 parasite genetic background should have an impact on the disease outcome.
85 Chagas disease is one of the main health problems in Latin America, causing
86 more than 10000 deaths per year, and incapacity in infected individuals [1].

87 In humans, the infection initiates with trypomastigotes deposited on
88 mucous or skin, along with triatomine bug faeces, when the insect vector feeds
89 on blood. Trypomastigotes are able to invade any nucleate cells at the infection
90 site. Once inside the cell, trypomastigotes differentiate to amastigotes, which are
91 the intracellular and replicative form. After several division cycles, amastigotes
92 differentiate again into trypomastigotes, the infected cells burst, and parasites

93 are released into the interstitial space. Trypomastigotes can either infect
94 neighboring cells or spread distantly by circulation. Successive cycles of
95 intracellular infection and replication followed by bloodstream trypomastigote
96 dissemination are the hallmark of the initial acute phase, which drives the
97 amplification of the parasitic load, and eventually produces the infection of
98 organs and tissues [2]. The acute phase ends approximately 2-3 months after
99 the initial infection, the time required by the host immune system to control
100 parasitemia and clear most trypomastigotes from peripheral circulation.
101 However, a chronic and persistent infection is already established, characterized
102 by the presence of intracellular amastigotes essentially confined into tissues
103 along with positive serologic tests [2,3].

104 The experimental murine model allowed to understand that during the
105 acute phase, trypomastigotes disseminate from the inoculation site to almost all
106 tissues, to render completely parasitized mice, few days after the initial infection
107 [4]. This entails that trypomastigotes should be able to escape from peripheral
108 circulation, cross the vascular endothelium and migrate through the extracellular
109 matrix (ECM) to establish a tissue intracellular infection [5]. The effectiveness of
110 trypomastigotes to cross biological barriers and migrate through tissues will
111 impact on *T. cruzi* ability to produce a severe, moderate or mild tissue infection.
112 This process -that can be linked to parasite virulence and dynamic of infection *in*
113 *vivo*- is poorly understood. Some authors suggested that the rupture of the
114 endothelial barrier is necessary for the infection of target tissues [6]. On the
115 contrary, others showed that trypomastigotes traverse the endothelial barrier
116 involving a transcellular traffic of trypomastigotes through endothelial cells,
117 mediated by the activation of the bradykinin receptor 2, and without disturbing its

118 integrity nor its permeability [7]. Since different combinations of parasite and
119 mouse strains present differential tissue colonization and target organs of
120 damage [8,9], the differences between both proposed transmigration models
121 could be attributed to the different strains employed. Either way, trypomastigote
122 transmigration through tissues is an essential event for *T. cruzi* infection. Studies
123 on *T. cruzi* transmigration have been very limited, probably because of the
124 extremely simplicity of monolayers cultures and –on the other hand- the
125 complexity of *in vivo* models, which present low spatio-temporal resolution.
126 Three-dimensional (3D) cultures are physiologically relevant and a good
127 alternative because they mimic the microarchitecture of tissues and can provide
128 an environment similar to the encountered in natural infections [10].

129 Spheroids are small aggregates of cells that do not adhere to a culture
130 substrate and grow in 3D. Cells interact with each other and secrete the
131 extracellular matrix (ECM) in which they reside, resembling their original
132 microenvironment both functionally and structurally [11,12]. Spheroids have
133 been broadly employed and deeply contribute to understand mechanisms in
134 cancer biology and immunology [13-15], but they have rarely been employed to
135 explore infectious diseases and host-parasite interactions. Remarkably, the co-
136 culture of spheroids of myocytes with *T. cruzi* trypomastigotes has demonstrated
137 to be an accurate model of fibrosis and hypertrophy that adequately recreates
138 the chronic chagasic cardiomyopathy [16,17]. In the present work we took
139 advantage of the 3D spheroid technology to disclose how trypomastigotes
140 transmigrate across tissues, which is a key process of the host-parasite interplay
141 in the early steps of infection. We demonstrate that the invasiveness of

142 trypomastigotes from different *T. cruzi* strains and isolates into spheroids can be
143 associated with their *in vivo* behavior and virulence.

144

145 **Materials and Methods**

146 **Reagents and sera**

147 Ultrapure Agarose, Carboxy-fluoresceinsuccinimidyl ester (CFSE) and
148 CellTrace™ Far Red (CTFR) were acquired from Invitrogen. Polyethylenimine
149 (PolyAr87-PEI) transfection reagent was obtained from FFyB (University of
150 Buenos Aires). Anti *T. cruzi* antisera developed in mice was generated in our
151 laboratory and used along with goat anti-mouse conjugated to Alexa-488 or
152 Alexa-647 (Molecular Probes).

153 **Parasites and conditioned media**

154 *T. cruzi* trypomastigotes from different strains and DTUs employed were:
155 SylvioX10, K98, Dm28, 193-733MM and 199-173BB (DTU TcI); Y (DTU TcII);
156 185-748BB and 186-401BB (DTU TcV) and RA and CL Brener (DTU TcVI). All
157 strains were DNA genotyped by PCR-RFLP of *TcSC5D* and *TcMK* genes (S1
158 Fig), as described [18].

159 Parasites were routinely maintained by *in vitro* cultures on Vero cells as
160 previously described [19], and trypomastigotes harvested from supernatants.

161 Culture-derived trypomastigotes were labeled with CellTrace™ CFSE as we
162 previously described [20]. Trypomastigotes were alternatively labelled with
163 CellTrace™ Far Red CTFR (5 μ M), essentially with the same protocol with slight

164 differences in the incubation time (20 min at 37°C, followed by the addition of 1
165 ml of complete medium and an additional incubation of 5 min at 37°C in the
166 dark). After labelling, the motility of parasites was controlled under light
167 microscope. The percentage of labelled parasites and the fluorescence intensity
168 of CFSE and CTFR was determined by flow cytometry.

169 *T. cruzi* derived conditioned medium (CM) was obtained by a previously
170 standardized protocol [21]. In brief, cell-derived trypomastigotes (100x10⁶) were
171 washed with PBS, resuspended in 1 ml of MEM without serum (or MEM without
172 parasites as control medium) and incubated for 6 h at 37°C in a 5% CO₂
173 humidified atmosphere. Then, parasites were pelleted by centrifugation and the
174 cell-free supernatant (containing both extracellular vesicles as well as vesicle-
175 free secreted material) was centrifuged twice for 10 min at 15000 xg. The
176 clarified supernatant was filtered through a 0.45 µm syringe filter, to obtain the
177 CM, which was aliquoted and stored at -70°C until use.

178 **Cell culture and stable HeLaR2 cell line generation**

179 Vero, HeLa and HEK293T cells were grown in MEM (Gibco) supplemented with
180 10% (v/v) fetal bovine serum (Natocor), 100 U/ml penicillin and 10 µg/ml
181 streptomycin. Cells were maintained at 37°C in 5% CO₂ and 95% air in a
182 humidified incubator. To obtain Hela cells stably expressing LifeAct-RFP,
183 permissive HEK293T cells were first employed to produce lentiviral particles
184 packed with LifeAct-RFP, essentially as described by Gerber *et al* [22]. Briefly,
185 HEK293T were seeded on 24-well plates (3x10⁴ cells/well) and transfected 24 h
186 later by the PEI method with a mix of 0.5 µg pCMV-dR8.9 DVpr (packaging
187 plasmid), 0.05 µg pCMV-VSV-G (envelope plasmid) and 0.5 µg of the pLenti

188 LifeAct-RFP (transfer plasmid) per well. The supernatant containing lentiviral
189 particles packed with LifeAct-RFP was collected at 48 and 72 h after
190 transfection, precleared, and concentrated by centrifugation. HeLa cells (3x10⁴
191 cells/well) were transduced in MEM containing 10% FBS with a 0.3 m.o.i. of
192 lentiviral particles, and expanded in culture flasks. Cells expressing LifeAct-RFP
193 (HeLaR) were sorted by flow cytometry, and cloned by limiting dilution. The
194 clone number 2 (HeLaR2) stably expressing LifeAct-RFP was selected and
195 employed for all the experiments.

196 **HeLa spheroids and infection model**

197 Spheroids of HeLaR2 cells were generated by the liquid overlay method [23].
198 Cells (1000/well) were added to U-bottom 96-well plates coated with agarose 1%
199 in PBS (w/v) and cultured in MEM 10% FBS. The formation of spheroids was
200 controlled by microscopy from 24 h post seeding (S2 Fig). At 72 h, each well
201 contained one spheroid of 300-400 μ m diameter, conformed by \approx 9000 cells.
202 For *T. cruzi* infection, twelve spheroids were placed on each well of an agarose
203 pre-coated p24 plate and incubated with 1 or 10 m.o.i. of trypomastigotes (or
204 control medium) for 1 or 24 h, in MEM supplemented with 4% FBS. When
205 appropriate, 100 μ l of medium was replaced by 100 μ l of CM. When indicated,
206 2D-monolayers of HeLaR2 cells (10x10⁵ cells/well) were incubated with 1 or 10
207 m.o.i. of trypomastigotes also labelled with CFSE in a final volume of 500 μ l of
208 MEM 4%.

209 For co-infection assays, 12 spheroids (in one p24 well) were simultaneously
210 incubated with CL Brener and SylvioX10 for 24 h with 10 m.o.i. of each *T. cruzi*
211 strain, labelled with a different stain.

212 **Cellular infection determined by flow cytometry**

213 Infected spheroids were collected in 1.5 ml tubes, washed three times with PBS
214 and disaggregated by addition of 200 μ l 0,25% trypsin/EDTA for 10 min at 37°C.
215 The cellular pellet -collected by centrifugation 10 min at 1000 x g- was washed
216 three times and fixed in PBS 0.5% PFA. Infected 2D-monolayer cells were
217 trypsinized and treated like 3D spheroids. Samples were acquired on a
218 FACSCalibur (Becton Dickinson); gated HeLaR2 by forward and side scatter
219 parameters were selected. A total of 10,000 events were analyzed for each
220 condition. FL1- cells represented uninfected HeLaR2 cells while FL1+
221 represented cells infected (either with intracellular parasites and/or attached to
222 cell membrane) with CFSE-labelled parasites, FL4+ cells were those infected
223 with CTFR-labelled parasites. Data was analyzed using FlowJo v10.0.7
224 software. Statistical significance was determined by two-tailed unpaired student *t*
225 *test* (Prism, GraphPad Software).

226 **Quantification of free-parasites inside spheroids**

227 Infected spheroids disaggregated by trypsin treatment were centrifuged for 10
228 min at 5700 x g to collect HeLaR2 cells and parasites that were infecting or
229 attached to HeLa cells, as well as parasites that were free inside spheroids (i.e.
230 not associated to cells but inside spheroids). The pellet was then analysed by
231 confocal microscopy to determine infected cells as well as free parasites
232 (expressed as number of free-parasites for each 100 HeLaR2 cells). Statistical
10

233 significance was determined by two-tailed unpaired student *t* test (Prism,
234 GraphPad Software).

235 **Parasitic load into spheroids**

236 The total cargo of parasites inside the spheroids, either infecting cells or free in
237 the ECM, was determined by qPCR. For doing so, each treatment was carried
238 out by duplicate: one sample was used to determine the parasite load
239 associated to spheroids (sample 1) while the other was used to determine the
240 total cargo of parasites in the well (sample 2: parasites associated to spheroids
241 plus parasites free in the medium/well). Infection was carried out as mentioned
242 above. After 24 h, spheroids from sample 1 were collected in 1,5 ml tubes and
243 carefully washed five times with sterile PBS to eliminate parasites from the
244 supernatant avoiding the disassembling of spheroids. Instead, for sample 2
245 spheroids and medium were collected together, centrifuged for 10 min at 5700 x
246 g and the pellet washed with sterile PBS. Samples were subjected to a standard
247 salting out protocol to obtain genomic DNA [24]. gDNA concentration was
248 measured using Nanodrop and 50 ng were used in each qPCR reaction, which
249 were carried out with Kapa Sybr Fast Universal Kit (Biosystems) in a 7500 Real
250 Time PCR System (Applied Biosystems). The *T. cruzi* single copy gene *PCD6*
251 (TcCLB.507099.50) was amplified with primers v099.50bFw
252 (CAGGCATCACCGTATTTCCA) and 099.50bRev
253 (CTCTTGTCCGTGCCAAACA) [25]. To determine *T. cruzi* DNA (TcDNA)
254 abundance, DNA content was normalized to human *GAPDH* gene (53MFZ-
255 GAPDHFw: ACCACCCTGTTGCTGTAGCCAAAT and 54MFZ-Rev:
256 GACCTGACCTGCCGTCTAGAAAAAA). Results were analysed with the LinReg

257 software [26]. The percentage of *TcDNA* inside spheroids was calculated as
258 $X\% = TcDNA_{sample1} \times 100 / TcDNA_{sample2}$ and expressed as mean \pm SD of three
259 independent experiments. Statistical significance was determined by student *t*
260 *test* (GraphPad software).

261 **Parasite invasiveness and dissemination**

262 Infected spheroids were fixed by adding PFA to a 3.2% final concentration and
263 incubated at 37°C for 1.5 h. Then, spheroids were washed with PBS as
264 described previously [20] and mounted. Fluorescence images were acquired
265 with a confocal Olympus FV1000 microscope. CFSE or CTFR labelled parasites
266 were imaged with a 488 nm or 647 nm laser, respectively, while HeLaR2 cells
267 were imaged at 530 nm. Z-stacks were collected with a 10x objective from 0 to
268 150 μ m in depth with 2 μ m intervals in the vertical z-axis. Alternatively, images
269 were acquired with a 40x objective, and the spheroid was scanned at 10, 30 and
270 50 μ m in depth from the surface. To determine the localization of parasites,
271 spheroids were analyzed with a 60x objective and Z-stacks were collected at 0.2
272 μ m intervals in the z-axis. All images were analyzed with ImageJ [27] software;
273 3D reconstructions and 3D-movies were generated with the 3D-viewer plugin.

274 **Electron microscopy**

275 Infected spheroids were fixed in 4% PFA and serially dehydrated with increasing
276 ethanol solutions (10-100 %) followed by critical point drying with carbon dioxide.
277 Samples were then coated with 60%/40% palladium/gold and acquired with a
278 scanning electron microscope (Philips - XL Serie 30).

279

280 **Free-swimming assay**

281 Trypomastigotes (15×10^6) were resuspended in 5 ml MEM 4% SFB, transferred
282 to round-bottom centrifuge tubes (Oak Ridge Style) and centrifuged at 2,500 x g
283 for 8 min, which resulted in parasites at the bottom of the tubes forming a thin
284 pellet. The tubes were then incubated 2 h at 37°C, to allow trypomastigotes to
285 freely swim. Aliquots of 1 ml were carefully taken from the top (layer 5) to the
286 bottom; the pellet was resuspended in 1 ml of medium. Parasites in each fraction
287 were enumerated by counting in a Neubauer chamber.

288 **Statistical analysis**

289 All statistical analyses and graphs were performed with GraphPad Prism 7
290 (GraphPad Software, USA). We used a two-tailed unpaired *t* test when the
291 means of two groups were compared. When more than 2 groups were
292 compared, we used two-way ANOVA with Bonferroni multiple comparison test.
293 Significant differences were designed when P-value (P) n.s. ≥ 0.05 , * $p < 0.05$,
294 ** $p < 0.01$, *** $p < 0.001$.

295

296 **Results**

297 ***T. cruzi* trypomastigotes are less infective in 3D spheroids than in 2D
298 monolayer cultures.**

299 *Trypanosoma cruzi* presents a high genetic heterogeneity and, currently,
300 *T. cruzi* strains are classified into six clusters or discrete typing units (DTUs),
301 named TcI to TcVI [28]. We selected CL Brener (DTU TcVI) and SylvioX10 (DTU
302 TcI) strains, of high and low virulence, respectively, and whose biologically
303 distinctive behavior in experimental models of *T. cruzi* infection is well

304 characterized [8,29-31].

305 HeLa cells constitutively expressing LifeAct-RFP (HelaR2 hereon), along
306 with trypomastigotes labelled with CFSE or CTFR were employed to monitor
307 short-time infection dynamics and host-parasite interactions (Fig 1). We first
308 evaluated the infection profile of trypomastigotes both on conventional 2D
309 monolayers and in 3D spheroids (Fig 2). While on conventional 2D monolayer
310 cultures CL Brener and SylvioX10 parasites showed similar infection rates
311 (~70%) (Fig 2A,C), both strains were much less effective to infect 3D spheroids
312 (Fig 2B,C) and with differences between both strains. Infection with CL Brener
313 rendered higher number of cells with cell-attached or internalized parasites
314 (38,2% CL Brener vs 8,5% SylvioX10), as detected by flow cytometry of
315 disaggregated spheroids (Fig 2B). The total cargo of parasites inside the
316 spheroids, which includes intracellular parasites, surface attached, as well as
317 free parasites migrating inside spheroids through the extracellular matrix, was
318 also higher on CL Brener than SylvioX10 infected spheroids (48% vs 18%,
319 determined by qPCR; Fig 2D). Differences between strains were also registered
320 when free-parasites (i.e. not associated to cells) inside spheroids were
321 enumerated (Fig 2E-F). Altogether, these results evidence that both strains have
322 different abilities to infect 3D cultures, being CL Brener strain 2-3 fold more
323 infectious than SylvioX10. These findings were also registered with different
324 multiplicity of infection, and contrast with the similar behavior of both strains on
325 monolayer cultures (S3 Fig).

326 **Trypomastigotes from different strains disseminate differentially inside**
327 **spheroids.**

328 A panoramic view of spheroids, reconstructed from confocal stacks shows that
329 SylvioX10 trypomastigotes were preferentially localized at the spheroid surface.
330 Parasites were mostly focalized in large clumps that resembled a “patch-like”
331 distribution pattern (Fig 3A, S1 movie). By contrast, CL Brener parasites were
332 evenly distributed all over the surface of spheroids (Fig 3B, S2 movie).

333 The transmigration and invasiveness of trypomastigotes was analyzed by
334 scanning the spheroids by confocal microscopy. Most SylvioX10 trypomastigotes
335 were retained at spheroid surface or at the first layers of cells, and only scarce
336 trypomastigotes were detected up to 30 μ m in depth (Fig 3C). On the other
337 hand, CL Brener parasites were able to deepen into spheroids: migrated
338 uniformly and were easily detected up to 50 μ m in depth (Fig 3D). The migration
339 through the spheroid seems to be a fast movement because similar patterns
340 were observed from 1 h post infection (S4 Fig). In brief, confocal scanning
341 evidenced that CL Brener trypomastigotes can efficiently transmigrate deeply
342 into spheroids, while SylvioX10 is retained at the surface, which corresponds
343 with the differential virulence of both strains.

344 **Trypomastigotes of high migratory CL Brener strain use a paracellular
345 migration route to move inside spheroids.**

346 To answer how trypomastigotes spread within spheroids, we analyzed the
347 parasite-spheroid interaction with higher resolution techniques, such as scanning
348 electron microscopy (SEM) and higher power snapshots by confocal
349 microscopy.

350 As evidenced by confocal microscopy, SEM images also showed numerous
351 SylvioX10 parasites attached to the surface of individual cells (Fig 4A, panels b,

352 c; white arrows). Notably, CL Brener trypomastigotes were predominantly caught
353 entering into spheroids through the space between cell-cell junctions (Fig 4A,
354 panels e, f; white asterisks). Spheroids infected with SylvioX10 also presented
355 multiple intracellular amastigotes in the superficial layers -first 10 μm - of cells
356 with an untidy distribution (Fig 4B panels a, b and c; 4C and S3 movie).
357 Confocal slices of spheroids infected with CL Brener made evident that there is
358 an orderly distribution pattern around cell-cell contacts (Fig 4B panels d, e, f;
359 white asterisks). At shorter times, CL Brener trypomastigotes were plainly
360 observed in the space between cells, on their way through the extracellular
361 matrix, suggesting a paracellular route of transmigration within the spheroid (Fig
362 4D and S4 and S5 movies). CL Brener trypomastigotes were also detected
363 intracellularly, though fastened to the cellular membrane (S6 movie).

364 **The capacity of transmigration is not transferable between strains.**

365 CL Brener and SylvioX10 strains presented not only dissimilar invasiveness
366 profiles, but also their allocation at the superficial layers of spheroids was very
367 distinctive (Fig 3 and 4). We then investigated if transmigration could be
368 transferred from the highly migrant CL Brener strain to the low migrant
369 SylvioX10, through soluble or secreted factors or by co-cultivation of both strains
370 (Fig 5). Interestingly, each strain retained its own dissemination pattern (Fig 5A)
371 and rate of infection (Fig 5B) irrespective of the presence (or absence) of the
372 other strain. Conditioned media (including both soluble and vesicle-contained
373 secreted factors) from CL Brener or SylvioX10 did not cause changes in the
374 invasiveness pattern or percentage of infected cells (S5 Fig). Together, these
375 results indicate that the transmigration capacity of *T. cruzi* is a strain-specific trait
376 that cannot be transferable by soluble or secreted factors, nor through co-

377 cultivation of migrant and non-migrant trypomastigotes.

378 **Transmigration deep inside spheroids can be linked to virulence.**

379 To evaluate if the differential transmigration profile could be linked to parasite
380 DTU or virulence, the transmigration into spheroids of other well characterized *T.*
381 *cruzi* strains was also analyzed. Low virulent strains (K98 and Dm28; Tcl)
382 presented low ability to transmigrate into spheroids (Fig 6). In contrast, virulent
383 strains (RA [TcVI] and Y [TcII]) showed a transmigration pattern resembling the
384 observed for CL Brener (Fig 6) (Fig 6A and S7 and 8 movies).

385 Finally, we analyzed the transmigration of four recent clinical isolates of *T. cruzi*.
386 One isolate was derived from a *T. cruzi*-infected mother that after several
387 pregnancies never delivered an infected child (isolate 773MM, Tcl; non-
388 congenital transmission). The other isolates, derived from babies that were born
389 congenitally infected (isolates 173BB, Tcl; 748BB, TcV; and 401BB, TcV;
390 congenital transmission) [32]. The non-congenital isolate (733MM) [32] showed
391 a low ability to migrate deep inside spheroids. Also, a “patch-like’ distribution
392 pattern, similar to the observed with SylvioX10 strain was observed (Fig 7B). In
393 contrast, congenitally isolated parasites presented a highly migrant phenotype.
394 Either DTU Tcl or TcV isolates from congenitally infected babies were found
395 deeply inside spheroids and easily visualized along the first 50 μm in depth (Fig
396 7A).

397 The cellular infection produced by 733MM was ~20%, a value near the one
398 registered with the low virulent SylvioX10 strain, while the 40% of infection of
399 cells in spheroids produced by congenital isolates resembled the infection
400 produced by CL Brener strain (Fig 7C).

401 Ultimately, because trypomastigotes of different strains behave differently when
402 they are allowed to swim freely in the medium, we analyzed parasite motility as a
403 possible trait linked to invasiveness within spheroids (S6 Fig). We consider a
404 strain (or isolate) as poor motile when more than 20% of the parasites remain at
405 the pellet in this assay. Although the swimming ability of SylvioX10 and CL
406 Brener strains were considerably different and agree with their behavior in
407 spheroids, other strains showed no association between the transmigration
408 inside spheroids and their swimming ability (for example, up to 60% of parasites
409 from 173BB and 401BB -congenital isolates highly migrant in spheroids-
410 remained between the pellet and layer 1).

411

412 **Discussion**

413 The infection with the protozoan parasite *Trypanosoma cruzi* evolves from
414 a short acute to a long lasting chronic phase when cardiac, neurological or
415 intestinal disorders become evident [3]. Although the pathology appears only at
416 the chronic phase, the infection of tissues initiates during acute phase and is the
417 consequence of the early dissemination of trypomastigotes. Indeed, *T. cruzi* can
418 disseminate and establish an intracellular infection in any tissue of the
419 mammalian host [5]. To accomplish this, trypomastigotes must migrate and
420 actively cross several biological barriers, from the initial infection site to the
421 target organs of damage, where parasites replicate intracellularly as amastigotes
422 [2]. Murine experimental models of *T. cruzi* infection have helped to understand
423 that some parasite strains present tropism for certain tissues or organs while
424 others are essentially pantropic and can colonize indistinctly any tissue [5,33,34].

425 Usually, pantropic strains are more virulent in the murine model. It can be
426 inferred that, since those strains colonize a broader range of tissues, they are
427 also more efficient in the transmigration process. However, how trypomastigotes
428 transmigrate, the mechanisms underlying this process and its significance in the
429 host-parasite interplay are poorly understood.

430 In this work, we employed 3D cultures to mimic the tisular
431 microarchitecture encountered by trypomastigotes in the mammalian host during
432 its *in vivo* life cycle. We studied the process of transmigration and dissemination
433 of the parasites across spheroids for the first time, and demonstrate a link
434 between 3D transmigration and *in vivo* behavior. Strains or isolates that are
435 more virulent *in vivo* (in natural or experimental infections) transmigrated deeper
436 inside spheroids than no virulent strains. In an *in vivo* infection, the ability to
437 transmigrate will favour pathogen dissemination into the host, at the same time
438 that parasites evade the immune system and increase the opportunity to find an
439 adequate microenvironment to settle for the tissular infection [35-38].

440 By employing the 3D spheroid model, we focused on one hand in the
441 ability of *T. cruzi* strains to infect mammalian cells (evaluated by flow cytometry
442 as cells with either internalized or attached parasites). On the other hand, we
443 also examined the invasiveness of trypomastigotes, which means how deep
444 inside the spheroids trypomastigotes are detected. Somehow both events
445 (invasiveness and infection) are linked by the fact that *T. cruzi* strains that were
446 highly migrant were also those that presented higher infection rates, probably
447 because the transmigration was a necessary step to infect the cells located deep
448 inside the spheroids. This fact can also explain why poorly migrant strains

449 presented low infection rates in the 3D model, irrespective of their accurate
450 infection rate in conventional 2D monolayer cultures. However, considering the
451 times at which transmigration was analyzed, it is unlikely that transmigration was
452 the result of cellular invasion and replication of parasites. We postulate the
453 transcellular and paracellular transmigration routes as two possible ways for
454 trypomastigotes to reach the deeper layers of spheroids. Even more, we
455 speculate that how *T. cruzi* transmigrates can be also a strain dependent trait
456 and that different strains or isolates can employ differential transmigration
457 strategies. Electronic microscopy images strongly suggest that CL Brener strain
458 goes through spheroids by a paracellular route, without crossing the cells but
459 between cell-cell junctions. Although the biological significance of this
460 transmigration strategy should be carefully studied, we hypothesize that the
461 paracellular route would allow the parasite to internalize into the tissues without
462 disrupting the cellular homeostasis and, therefore, without triggering an
463 inflammatory response. Moreover, a paracellular route would be a faster
464 transmigration mechanism for trypomastigotes to find their target allocation
465 inside tissues, without the need to invade and replicate intracellularly. In line with
466 these results, Coates et al (2013) showed that *T. cruzi* trypomastigotes can
467 cross a monolayer of endothelial cells without cell damage. They suggested that
468 this process might be mediated by the protease cruzipain, which can convert
469 kininogen to bradykinin (involved in endothelial permeability) [7]. The picture of
470 trypomastigotes distribution was very distinctive between CL Brener and
471 SylvioX10 strains, even from the initial steps of interaction with mammalian cells
472 in our 3D model. While CL Brener trypomastigotes are regularly distributed and
473 positioned in between cell-cell junctions on the external layers of the spheroid

474 surface, SylvioX10 trypomastigotes are grouped in patches of several parasites
475 stuck over the cells. Previous works with *Trypanosoma brucei* evidenced that
476 trypomastigotes can cross the blood brain barrier both by transcellular and
477 paracellular routes, promoting the expression of ICAM-1 and VCAM-1 [39-41].
478 On the other hand, *T. gondii* employs a paracellular route for tissue
479 transmigration, through the interaction between TgMIC2 and host occludins from
480 TJs and ICAM-1[42,43]. Interference with the transmigration process avoids *in*
481 *vivo* infectivity both in *T. gondii* and *P. falciparum* [44,45]. Interestingly, the loss
482 of genes associated with transmigration in *P. falciparum* did not impair cellular
483 invasion, supporting the idea that tissue invasiveness and cellular infection can
484 be two independent processes [45].

485 Trypomastigote's motility can be understood as its ability to present a
486 directional movement, which in turn could impact on the cellular infection rates.
487 We found a pronounced difference in swimming motility between SylvioX10 (low
488 migrant and low motile) and CL Brener (high migrant and high motile)
489 trypomastigotes. However, analyses of a broader panel of strains demonstrated
490 that transmigration cannot be solely explained by the motile ability of
491 trypomastigotes. Presumably, transmigration depends both on motility and
492 migration of the parasite as well as on its interaction with the surrounding
493 microenvironment. In this sense, Barragan *et al*, (2002) showed that a high
494 migration rate of *T. gondii* is associated with a highly virulent phenotype [46].
495 Indeed, correlation between high virulent strains and congenital toxoplasmosis
496 has also been noted [47,48]. On the other hand, Éva Dóró et al (2019) have very
497 recently evaluated the migration of trypomastigotes of *T. carassii* in an *in vivo*
498 model. This awesome work clearly shows that the movement of parasites inside

499 zebrafish occurs through the interstitial space and how its density and
500 compaction determines the direction of trypomastigotes migration [49].

501 During congenital transmission of *T. cruzi* infection, trypomastigotes must
502 cross epithelial and connective tissues that compose the placental barrier to gain
503 access to and infect the fetus. Therefore, transplacental infection is another
504 aspect of *T. cruzi*-host interplay that is associated with parasite transmigration.
505 We have characterized the invasiveness inside spheroids of isolates recently
506 obtained from babies born with congenital Chagas disease. We demonstrated
507 that the congenital isolates were highly invasive into spheroids, in contrast with
508 the isolate obtained from a mother, which after delivered several children never
509 transmitted the infection to her offspring, which showed a low/moderate
510 transmigration ability. *T. cruzi* congenital transmission is the result of a complex
511 interaction between trypomastigotes and the placental barrier [50-52]. Recently,
512 Juiz et al (2017) described a differential placental gene response induced by
513 strains with different tropism and virulence. They reported that a strain that was
514 isolated from a human case of congenital infection (VD) presented higher
515 tropism by the murine placenta than a non-virulent and myotropic strain (K-98)
516 [53]. In our 3D model, K-98 strain showed a low migrant phenotype. Although we
517 did not analyze the transmigration profile of VD strain, all the congenital isolates
518 assayed here were highly migrant.

519 The intratissular migration is key during the development of metastasis
520 and it has been approached in several studies on cancer [54]. Tumoral cells
521 produce and prompt to the secretion of cytokines and proteases that will favour
522 the migration across different biological barriers. Proteases are necessary to

523 disrupt cell-cell junctions, extracellular matrix and the basal lamina [55]. Although
524 little is known about the transmigration process in host-pathogen interactions,
525 the secretion of proteases could also be required to disrupt intercellular junctions
526 and extracellular matrix for *T. cruzi* transmigration. However, in our experimental
527 conditions, the invasiveness was not a transferable feature between strains,
528 neither by soluble or secreted factors nor by co-cultivation of invasive and non-
529 invasive trypomastigotes. This observation suggests that unsecreted and strain
530 specific factors are required to transmigrate into the spheroids, while it does not
531 exclude the involvement of proteases and other soluble factors. Differentially-
532 expressed and/or strain specific membrane-associated molecules from
533 trypomastigotes might be targets to be evaluated in the near future.

534 Altogether, our results demonstrated that in a 3D microenvironment each
535 strain presents a characteristic migration pattern and tissular distribution that
536 could be associated to their *in vivo* behavior. Our work also validates the
537 accuracy and utility of the 3D spheroid model to study complex host-parasite
538 interactions. Certainly, the findings presented here could not have been studied
539 with traditional 2D monolayer cultures.

540

541 **Acknowledgements**

542 We acknowledge L. Sferco and A. Chidichimo for technical assistance
543 with *in vitro* parasite cultures, and V. Campo and G.V. Levy for advice in qPCR
544 assays. We are grateful to A.M.M. Massaldi for checking the English version of
545 the manuscript. This work was supported by grants from Agencia Nacional de

546 Promoción Científica y Tecnológica / Fondo para la Investigación Científica y
547 Tecnológica -ANPCyT/FONCyT- (PICT-2016-0108 to VT and PICT 2017-2644
548 to MER) from Argentina. The funders had no role in study design, data collection
549 and analysis, decision to publish, or preparation of the manuscript.

550

551 **References**

- 552 1. OPS OMS | Enfermedad de Chagas. 2015. Available from:
553 http://www.paho.org/hq/index.php?option=com_topics&view=article&id=10&Itemid=40743&lang=es
- 555 2. Andrade LO, Andrews NW. Opinion: The *Trypanosoma cruzi*–host-cell
556 interplay: location, invasion, retention. *Nat Rev Microbiol*. 2005; 3(10):819–
557 23.
- 558 3. Rassi A, Rassi A, Marin-Neto JA, al. et, al. et, Guillen I de. Chagas
559 disease. *Lancet*. 2010; 375(9723):1388–402.
- 560 4. Lewis MD, Francisco AF, Taylor MC, Jayawardhana S, Kelly JM. Host and
561 parasite genetics shape a link between *Trypanosoma cruzi* infection
562 dynamics and chronic cardiomyopathy. *Cell Microbiol* 2016; 18(10):1429–
563 43.
- 564 5. Costa FC, Francisco AF, Jayawardhana S, Calderano SG, Lewis MD,
565 Olmo F, et al. Expanding the toolbox for *Trypanosoma cruzi*: A parasite line
566 incorporating a bioluminescence-fluorescence dual reporter and
567 streamlined CRISPR/Cas9 functionality for rapid *in vivo* localisation and
568 phenotyping. *PLoS Negl Trop Dis*. 2018; 12(4):e0006388.

569 6. Prado CM, Jelicks LA, Weiss LM, Factor SM, Tanowitz HB, Rossi MA. The
570 vasculature in chagas disease. *Adv Parasitol.* 2011; 76:83–99.

571 7. Coates BM, Sullivan DP, Makanji MY, Du NY, Olson CL, Muller WA, et al.
572 Endothelial Transmigration by *Trypanosoma cruzi*. *PLoS One.* 2013;
573 8(12):e81187.

574 8. Lewis MD, Fortes Francisco A, Taylor MC, Burrell-Saward H, McLatchie
575 AP, Miles MA, et al. Bioluminescence imaging of chronic *Trypanosoma*
576 *cruzi* infections reveals tissue-specific parasite dynamics and heart disease
577 in the absence of locally persistent infection. *Cell Microbiol.* 2014;
578 16(9):1285–300.

579 9. Santi-Rocca J, Gironès N, Fresno M. Multi-Parametric Evaluation of
580 Trypanosoma cruzi Infection Outcome in Animal Models. In: *Methods in*
581 *molecular biology* (Clifton, NJ). 2019. p. 187–202.

582 10. Shamir ER, Ewald AJ. Three-dimensional organotypic culture: experimental
583 models of mammalian biology and disease. *Nat Rev Mol Cell Biol.* 2014;
584 15(10):647–64.

585 11. Fennema E, Rivron N, Rouwkema J, van Blitterswijk C, de Boer J.
586 Spheroid culture as a tool for creating 3D complex tissues. *Trends*
587 *Biotechnol.* 2013; 31(2):108–15.

588 12. Zanoni M, Piccinini F, Arienti C, Zamagni A, Santi S, Polico R, et al. 3D
589 tumor spheroid models for *in vitro* therapeutic screening: a systematic
590 approach to enhance the biological relevance of data obtained. *Sci Rep.*
591 2016; 6(1):19103.

592 13. Baruzzi A, Remelli S, Lorenzetto E, Sega M, Chignola R, Berton G. Sos1
593 Regulates Macrophage Podosome Assembly and Macrophage Invasive
594 Capacity. *J Immunol.* 2015; 195(10):4900–12.

595 14. Röhland S, Wechselberger A, Spitzweg C, Huss R, Nelson PJ, Harz H.
596 Quantification of in vitro mesenchymal stem cell invasion into tumor
597 spheroids using selective plane illumination microscopy. *J Biomed Opt.*
598 2015; 20(4):040501.

599 15. Giannattasio A, Weil S, Kloess S, Ansari N, Stelzer EHK, Cerwenka A, et
600 al. Cytotoxicity and infiltration of human NK cells in in vivo-like tumor
601 spheroids. *BMC Cancer.* 2015; 15(1):351.

602 16. Garzoni LR, Adesse D, Soares MJ, Rossi MID, Borojevic R, Meirelles M de
603 NL de. Fibrosis and Hypertrophy Induced by *Trypanosoma cruzi* in a
604 Three-Dimensional Cardiomyocyte-Culture System. *J Infect Dis.* 2008;
605 197(6):906–15.

606 17. M. Ferrão P, M. Nisimura L, C. Moreira O, G. Land M, Pereira MC, de
607 Mendonça-Lima L, et al. Inhibition of TGF- β pathway reverts extracellular
608 matrix remodeling in *T. cruzi* -infected cardiac spheroids. *Exp Cell Res.*
609 2018; 362(2):260–7.

610 18. Cosentino RO, Agüero F. A Simple Strain Typing Assay for *Trypanosoma*
611 *cruzi*: Discrimination of Major Evolutionary Lineages from a Single
612 Amplification Product. *PLoS Negl Trop Dis.* 2012; 6(7):e1777.

613 19. Bernabó G, Levy G, Ziliani M, Caeiro LD, Sánchez DO, Tekiel V. TcTASV-
614 C, a Protein Family in *Trypanosoma cruzi* that Is Predominantly
615 Trypomastigote-Stage Specific and Secreted to the Medium. *PLoS One.*

616 2013; 8(7):e71192.

617 20. Rodríguez ME, Rizzi M, Caeiro L, Masip Y, Sánchez DO, Tekiel V.
618 Transmigration of *Trypanosoma cruzi* Trypomastigotes through 3D
619 Spheroids Mimicking Host Tissues. In: Methods in molecular biology
620 (Clifton, NJ). 2019. p. 165–77.

621 21. Caeiro LD, Alba-Soto CD, Rizzi M, Solana ME, Rodriguez G, Chidichimo
622 AM, et al. The protein family TcTASV-C is a novel *Trypanosoma cruzi*
623 virulence factor secreted in extracellular vesicles by trypomastigotes and
624 highly expressed in bloodstream forms. PLoS Negl Trop Dis. 2018;
625 12(5):e0006475.

626 22. Gerber PP, Cabrini M, Jancic C, Paoletti L, Banchio C, von Bilderling C, et
627 al. Rab27a controls HIV-1 assembly by regulating plasma membrane levels
628 of phosphatidylinositol 4,5-bisphosphate. J Cell Biol. 2015; 209(3):435–52.

629 23. Carlsson J, Yuhas JM. Liquid-overlay culture of cellular spheroids. Recent
630 Results Cancer Res. 1984; 95:1–23.

631 24. Miller SA, Dykes DD, Polesky HF. A simple salting out procedure for
632 extracting DNA from human nucleated cells. Nucleic Acids Res. 1988;
633 16(3):1215.

634 25. Campo VA. Comparative effects of histone deacetylases inhibitors and
635 resveratrol on *Trypanosoma cruzi* replication, differentiation, infectivity and
636 gene expression. Int J Parasitol Drugs drug Resist. 2017; 7(1):23–33.

637 26. Ramakers C, Ruijter JM, Deprez RHL, Moorman AF. Assumption-free
638 analysis of quantitative real-time polymerase chain reaction (PCR) data.

639 Neurosci Lett. 2003; 339(1):62–6.

640 27. Schneider CA, Rasband WS, Eliceiri KW. NIH Image to ImageJ: 25 years
641 of image analysis. Nat Methods. 2012; 9(7):671–5.

642 28. Zingales B, Miles MA, Campbell DA, Tibayrenc M, Macedo AM, Teixeira
643 MMG, et al. The revised *Trypanosoma cruzi* subspecific nomenclature:
644 Rationale, epidemiological relevance and research applications. Infect
645 Genet Evol. 2012; 12(2):240–53.

646 29. Marinho CRF, Nuñez-Apaza LN, Bortoluci KR, Bombeiro AL, Bucci DZ,
647 Grisotto MG, et al. Infection by the Sylvio X10/4 clone of *Trypanosoma*
648 *cruzi*: relevance of a low-virulence model of Chagas' disease. Microbes
649 Infect. 2009; 11(13):1037–45.

650 30. Marinho CRF, Nuñez-Apaza LN, Martins-Santos R, Bastos KRB, Bombeiro
651 AL, Bucci DZ, et al. IFN-gamma, But Not Nitric Oxide or Specific IgG, is
652 Essential for the In vivo Control of Low-virulence Sylvio X10/4
653 *Trypanosoma cruzi* Parasites. Scand J Immunol. 2007; 66(2–3):297–308.

654 31. Belew AT, Junqueira C, Rodrigues-Luiz GF, Valente BM, Oliveira AER,
655 Polidoro RB, et al. Comparative transcriptome profiling of virulent and non-
656 virulent *Trypanosoma cruzi* underlines the role of surface proteins during
657 infection. PLoS Pathog. 2017; 13(12):e1006767.

658 32. Volta BJ, Bustos PL, Cardoni RL, De Rissio AM, Laucella SA, Bua J.
659 Serum Cytokines as Biomarkers of Early *Trypanosoma cruzi* infection by
660 Congenital Exposure. J Immunol. 2016; 196(11):4596–602.

661 33. Santi-Rocca J, Gironès N, Fresno M. Multi-Parametric Evaluation of

662 Trypanosoma cruzi Infection Outcome in Animal Models. 2019. p. 187–202.

663 34. Lewis MD, Francisco AF, Taylor MC, Kelly JM. A New Experimental Model
664 for Assessing Drug Efficacy against Trypanosoma cruzi Infection Based on
665 Highly Sensitive In Vivo Imaging. *J Biomol Screen*. 2015; 20(1):36–43.

666 35. Harker KS, Ueno N, Lodoen MB. Toxoplasma gondii dissemination: a
667 parasite's journey through the infected host. *Parasite Immunol*. 2015;
668 37(3):141–9.

669 36. Kumar H, Tolia NH. Getting in: The structural biology of malaria invasion.
670 *PLOS Pathog*. 2019; 15(9):e1007943.

671 37. Drewry LL, Sibley LD. The hitchhiker's guide to parasite dissemination. *Cell*
672 *Microbiol*. 2019; e13070.

673 38. Lambert H, Barragan A. Modelling parasite dissemination: host cell
674 subversion and immune evasion by Toxoplasma gondii. *Cell Microbiol*.
675 2010 Mar; 12(3):292–300.

676 39. Mulenga C, Mhlanga JD, Kristensson K, Robertson B. Trypanosoma brucei
677 brucei crosses the blood-brain barrier while tight junction proteins are
678 preserved in a rat chronic disease model. *Neuropathol Appl Neurobiol*.
679 2001; 27(1):77–85.

680 40. Grab DJ, Nikolskaia O, Kim Y V., Lonsdale-Eccles JD, Ito S, Hara T, et al.
681 African trypanosome interactions with an in vitro model of the human blood-
682 brain barrier. *J Parasitol*. 2004; 90(5):970–9.

683 41. Nikolskaia O V., de A Lima APC, Kim Y V, Lonsdale-Eccles JD, Fukuma T,
684 Scharfstein J, et al. Blood-brain barrier traversal by African trypanosomes

685 requires calcium signaling induced by parasite cysteine protease. *J Clin*
686 *Invest.* 2006; 116(10):2739–47.

687 42. Weight CM, Jones EJ, Horn N, Wellner N, Carding SR. Elucidating
688 pathways of *Toxoplasma gondii* invasion in the gastrointestinal tract:
689 involvement of the tight junction protein occludin. *Microbes Infect.* 2015;
690 17(10):698–709.

691 43. Barragan A, Brossier F, Sibley LD. Transepithelial migration of *Toxoplasma*
692 *gondii* involves an interaction of intercellular adhesion molecule 1 (ICAM-1)
693 with the parasite adhesin MIC2. *Cell Microbiol.* 2005; 7(4):561–8.

694 44. Huynh M-H, Carruthers VB. *Toxoplasma MIC2* Is a Major Determinant of
695 Invasion and Virulence. *PLoS Pathog.* 2006; 2(8):e84.

696 45. Yang ASP, O'Neill MT, Jennison C, Lopaticki S, Allison CC, Armistead JS,
697 et al. Cell Traversal Activity Is Important for *Plasmodium falciparum* Liver
698 Infection in Humanized Mice. *Cell Rep.* 2017; 18(13):3105–16.

699 46. Barragan A, Sibley LD. Transepithelial migration of *Toxoplasma gondii* is
700 linked to parasite motility and virulence. *J Exp Med.* 2002 Jun
701 17;195(12):1625–33.

702 47. Howe DK, Sibley LD. *Toxoplasma gondii* Comprises Three Clonal
703 Lineages: Correlation of Parasite Genotype with Human Disease. *J Infect*
704 *Dis.* 1995; 172(6):1561–6.

705 48. Fuentes I, Rubio JM, Ramirez C, Alvar J. Genotypic Characterization of
706 *Toxoplasma gondii* Strains Associated with Human Toxoplasmosis in
707 Spain: Direct Analysis from Clinical Samples. *J Clin Microbiol.* 2001;

708 39(4):1566–70.

709 49. Dóró É, Jacobs SH, Hammond FR, Schipper H, Pieters RP, Carrington M,
710 et al. Visualizing trypanosomes in a vertebrate host reveals novel
711 swimming behaviours, adaptations and attachment mechanisms. *Elife*.
712 2019; 8. e48388.

713 50. Castillo C, Carrillo I, Libisch G, Juiz N, Schijman A, Robello C, et al. Host-
714 parasite interaction: changes in human placental gene expression induced
715 by *Trypanosoma cruzi*. *Parasit Vectors*. 2018;11(1):479.

716 51. Juiz NA, Torrejón I, Burgos M, Torres AMF, Duffy T, Cayo NM, et al.
717 Alterations in Placental Gene Expression of Pregnant Women with Chronic
718 Chagas Disease. *Am J Pathol*. 2018; 188(6):1345–53.

719 52. Bustos PL, Milduberger N, Volta BJ, Perrone AE, Laucella SA, Bua J.
720 *Trypanosoma cruzi* Infection at the Maternal-Fetal Interface: Implications of
721 Parasite Load in the Congenital Transmission and Challenges in the
722 Diagnosis of Infected Newborns. *Front Microbiol*. 2019; 10:1250.

723 53. Juiz NA, Solana ME, Acevedo GR, Benatar AF, Ramirez JC, da Costa PA,
724 et al. Different genotypes of *Trypanosoma cruzi* prod1. Juiz NA, Solana
725 ME, Acevedo GR, Benatar AF, Ramirez JC, da Costa PA, et al. Different
726 genotypes of *Trypanosoma cruzi* produce distinctive placental environment
727 genetic response in chronic experimental infecti. *PLoS Negl Trop Dis*.
728 2017; 11(3):e0005436.

729 54. Stuelten CH, Parent CA, Montell DJ. Cell motility in cancer invasion and
730 metastasis: insights from simple model organisms. *Nat Rev Cancer*. 2018;
731 18(5):296–312.

732 55. Wolf K, Friedl P. Extracellular matrix determinants of proteolytic and non-
733 proteolytic cell migration. *Trends Cell Biol.* 2011; 21(12):736–44.

734

735

736 **Figure captions**

737 **Fig 1. Model setup.**

738 (A) *Trypanosoma cruzi* SylvioX10 (DTU Tcl) and CL Brener (DTU TcVI)
739 trypomastigotes were labelled with CFSE: fluorescent images (left panel) and
740 quantification by flow cytometry (right panel). Black histograms: non-labelled
741 parasites; green histograms: CFSE labelled parasites. NS: Negative Staining.
742 (B) Spheroid of HeLaR2 cells at 72 h post seeding. Scale bar = 100 μ m.

743

744 **Fig 2. Differential ability of SylvioX10 and CL Brener trypomastigotes to**
745 **infect 2D-monolayer vs 3D-spheroid cultures.**

746 HeLaR2 (grown as monolayers or as spheroids, see Material and Methods
747 section) were incubated with 10 m.o.i. of CFSE-labelled CL Brener or SylvioX10
748 trypomastigotes or non-infected (control). (A, B) At 24 h post infection, cells
749 were trypsinized and the rate of infected HeLaR2 cells (either with internalized or
750 attached parasites) was determined by flow cytometry. (C) Quantification of
751 three independent experiments carried out as described for A and B. (D)
752 Quantification of the total parasite cargo inside spheroids, which includes both
753 cell-associated parasites and free parasites inside spheroids from three
754 independent experiments. At 24 h post infection either intact spheroids or the

755 whole content of the well (intact spheroids plus culture media with non-
756 internalized parasites) were harvested and total DNA purified. Parasite content
757 was estimated on the basis of qPCR of a single copy *T. cruzi* gene (*PCD6*,
758 TriTryp gene ID: TcCLB.507099.50). Percentage of *T. cruzi* DNA inside
759 spheroids respect to total *T. cruzi* DNA in the well was calculated. (E) Free
760 parasites inside spheroids infected with CL Brener or SylviX10, at 24 h p.i.
761 Representative confocal images of disaggregated spheroids, white arrows:
762 magnified cells; white asterisks: free parasites. (F) Quantification of free
763 parasites released from disaggregated spheroids. Data expressed as number of
764 free-parasites for each 100 HeLaR2 cells. Graphs represent the mean \pm SD of
765 three independent experiments *t test*, *p<0.05, **p<0.01, ***p<0.001.

766

767 **Fig 3. Differential dissemination pattern within spheroids of different**
768 **strains of *T. cruzi*.**

769 (A and B). 3D reconstruction of HeLaR2 spheroids infected with CFSE-
770 SylvioX10 or CFSE-CL Brener trypomastigotes. Z-stack images were obtained
771 by confocal microscopy. The distribution on the surface (X-Y left image), the
772 side plane (Z-Y middle image) and inside the spheroid (Y-X right image,
773 transversal view) are shown. Green: CFSE-trypomastigotes. Red: LifeAct-RFP
774 of HeLa cells. (C and D) Representative images of three confocal planes
775 obtained at 10, 30 and 50 μ m in depth on the z axis (40x objective). The detailed
776 distribution pattern of parasites is observed -green fluorescence-. Scale bar: 100
777 μ m.

778

779 **Fig 4. Differential host cell-parasite interaction pattern of different strains**

780 **of *T. cruzi* on the spheroid surface.**

781 Spheroids were cultured with CFSE-SylvioX10 or CFSE-CL Brener. (A) Cell-
782 parasite interaction on the surface of infected spheroids after 24 h of infection.
783 SEM microscopy showing the whole surface of infected spheroids (images a and
784 d) or detailed cell-parasite interactions (b-c for SylvioX10 and e-f for CL Brener)
785 are shown. White arrows show groups of parasites on the surface of SylvioX10
786 infected spheroids. White asterisks show CL Brener parasites located in the site
787 of cell cell-cell contact. Scale bar for a and d: 100 μ m; b and c: 10 μ m; d: 100
788 μ m; e: 10 μ m; f: 5 μ m. (B) Confocal microscopy capturing cell infection at 10 μ m
789 of infected spheroids with 60x objective. The distribution pattern of parasites on
790 the surface of infected spheroids is observed in a and d images for SylvioX10
791 and CL Brener, respectively. Blue arrows show magnified insets (b-c for
792 SylvioX10 and e-f for CL Brener). Yellow asterisks show multi-infected cells.
793 White asterisks show cell-cell contact associated parasites. Scale bar = 15 μ m.
794 (C) Multi-infected cell on the surface of SylvioX10 infected spheroids was
795 reconstructed in 3D. Multiple intracellular amastigotes can be observed. (D)
796 Spheroids of HeLaR2 cells were incubated with CFSE-CL Brener
797 trypomastigotes for 1h and then photographed by confocal microscopy. CFSE-
798 trypomastigotes in the paracellular space both in fluorescence images (a) as well
799 as in bright light (b) are shown. Scale bar 15 μ m.

800

801 **Fig 5. Invasiveness within spheroid is an intrinsic feature of each strain,**
802 **not complemented in trans.**

803 Spheroids of HeLaR2 cells were incubated with CFSE-CL Brener, CTFR-CL
804 Brener, CFSE-SylvioX10 or CTFR-SylvioX10 or simultaneously co-incubated
805 with both strains labelled with different dyes. (A) Representatives images of
806 three confocal planes obtained at 10, 30 and 50 μ m in depth -on the z axis- with
807 a 40x objective. Cyan: CTFR-SylvioX10; green: CFSE-CL Brener; red: HeLaR2
808 cells. Magnified insets (a-d) are shown in the right panels. Scale bar = 100 μ m.
809 (B) The same assay as described in A but spheroids were disaggregated and
810 cells with either attached or internalized parasites were quantified by flow
811 cytometry. Infections with one (mono-infections) or both strains simultaneously
812 (co-infections) were carried out also with interchanged dyes. The percentage of
813 infected cells was significantly different between SylvioX10 and CL Brener
814 parasites in all conditions tested. On the other hand, no differences in the
815 infection rate for each strain, both with the use of different staining dyes, as well
816 as, during the mono infections versus the co-infections were observed. Graphs
817 represent the mean \pm SD of three independent experiments. Data were analyzed
818 by one-way ANOVA followed by Bonferroni's multiple comparison test.

819

820 **Fig 6. The capacity of dissemination is linked to virulence.**

821 Spheroids of HeLaR2 cells were incubated with k98, Dm28c, Y or RA strains for
822 24 h. Three confocal planes were obtained at 10, 30 and 50 μ m in depth -on the
823 z axis- with 40x objective. The detailed distribution pattern of parasites is
824 observed. 3D-reconstruction is shown in lower panels. Green: CFSE labeled
825 parasites. Red: LifeAct-RFP. Scale bar = 100 μ m.

826

827 **Fig 7. Congenital trypomastigotes are more invasive and infective than**
828 **non-congenital parasites.**

829 Spheroids of HeLaR2 cells were incubated with 733MM, 173BB, 401BB or
830 748BB recent clinical isolates for 24 h. (A) Confocal planes were obtained at 10,
831 30 and 50 μ m in depth -on the z axis- with 40x objective. The detailed
832 distribution pattern of parasites is observed. Scale bar = 100 μ m. (B) Three-D-
833 reconstruction of infected spheroids with each strain is shown. Green: CFSE
834 labeled parasites. Red: LifeAct-RFP. (C) Percentage of infected HeLaR2 cells to
835 compare infectivity of non-congenital vs congenital isolated. Pink and blue bars
836 show SylvioX10 and CL Brener % of infection, respectively, as comparison
837 points. Graphs represent the mean \pm SD of three independent experiments.

838

839 **Supporting information captions**

840

841 **S1 Fig. Genotyping of *T. cruzi* strains and isolates** (according to Cossentino
842 et al, 2012).

843 (A) TcSC5D amplification product was digested with SphI/HpaI restriction
844 enzymes and fragments resolved in 2% agarose gels. Fragment length
845 polymorphism defined lineages TcI for SylvioX10, K98, 733MM and 173BB; TcII
846 for Y; TcV/VI for CL Brener, RA, 401BB and 748BB. (B) The digestion of TcMK
847 product with XbaI allows to distinguish between DTUs TcV (401BB and 748BB)
848 and TcVI (CL Brener and RA).

849

850 **S2 Fig. The 3D culture model.**

851 (A) Monolayer of HeLa cells stably expressing LifeAct-RFP (HeLaR2), generated
852 by lentiviral infection of the parental HeLa cells. (B) Spheroids formation by liquid
853 overlay. After 24 h, spheroids are irregular aggregates of cells. From 72 h after
854 culturing, spheroids seem to be compact aggregate of cells with well delimited
855 borders.

856

857 **S3 Fig. Infection of 2D-monolayer and spheroids at m.o.i. 1, with strains CL**
858 **Brener and Sylvio.**

859 HeLaR2 cells were incubated with CFSE-labelled trypomastigotes for 24 h and
860 then monolayers or spheroid cultures fixed. (A) the Infected cells were
861 determined by flow cytometry, which detects both attached and internalized
862 parasites. (B) Quantification of 3 independent experiments, carried out as
863 described for A. (C, D) Spheroids were disaggregated and released parasites
864 (free parasites inside spheroids) were visualized by fluorescence microscopy
865 and quantified. * *t test* <0.05.

866

867 **S4 Fig. Dissemination pattern within spheroids of CL Brener after 1 h of**
868 **infection.**

869 Spheroids incubated with 10 m.o.i. of CFSE-CL Brener parasites for 1h were
870 fixed and confocal planes were obtained at 10, 30 and 50 μm in depth -on the z
871 axis- with 40x objective. Representative images of the invasiveness of CL
872 Brener parasites -green fluorescence- that were detected even at 50 μm in depth
873 within the spheroids. Scale bar = 100 μm .

874

875 **S5 Fig. Invasiveness within spheroid is not mediated by soluble factors.**

876 (A) spheroids were incubated with CFSE-CL Brener (left) or CFSE-SylvioX10
877 (right) trypomastigotes for 24 h along with control media, or conditioned media
878 (CM) from either SylvioX10 or CL Brener trypomastigotes. Then, spheroids were
879 fixed and confocal images were taken at 10, 30 and 50 μ m in depth from
880 spheroid surface. (B) Spheroids incubated with CL Brener or SylvioX10
881 trypomastigotes in presence of control media or conditioned media were
882 disaggregated with trypsin and % of infected cells was measured by flow
883 cytometry.

884

885 **S6 Fig. The free motility *in vitro* is not associated with invasion inside**
886 **spheroids.** Trypomastigotes were pelleted in round bottom tubes and then
887 incubated for 2 h at 37°C in medium to allow free-swimming (Left image).
888 Aliquots of 1 ml (layer 1 to 5) of the medium from top to bottom were carefully
889 collected and quantification of the % of parasites in each layer and pellet was
890 carried out by microscopy, on Neubauer chamber (graph). Isolates / strains are
891 classified in two groups: those that presented low motility [>40 % of
892 trypomastigotes in the pellet after 2 h] and those with high motility [<20% of
893 parasites in the pellet] and trypomastigotes were homogeneously distributed
894 among all layers]. As a reference, the low migran strains (into spheroids) are in
895 pink and the high migrants are in sky blue. pasa a suplementaria

896

897 **S1 and S2 movies.**

898 HeLaR2 spheroid infected with CFSE-SylvioX10 (video1) or CFSE-CL Brener
38

899 (video 2); 3D reconstruction. Z-stack images were obtained by confocal
900 microscopy using 10x objective. The videos were realized by using ImageJ
901 software -3D viewer plugin-. Half of an infected spheroid rotating on the Y axis is
902 shown. Green: CFSE-parasites. Red: LifeAct-RFP of HeLa cells.

903

904 **S3 movie.**

905 3D reconstruction of a single HeLaR2 cell on the surface of a SylvioX10-infected
906 spheroid. Z-stack images were obtained by confocal microscopy using 60x
907 objective. The video was realized by using ImageJ software -3D viewer plugin-.
908 Multiple amastigotes within a single cell are shown. Green: CFSE-parasites.
909 Red: LifeAct-RFP of HeLa cells.

910

911 **S4 movie.**

912 3D reconstruction of a single CL Brener trypomastigote located inside the
913 spheroid ($\approx 30 \mu\text{m}$ deep) after 1 h of incubation. Z-stack images were obtained
914 by confocal microscopy using 60x objective. The video was realized by using
915 ImageJ software -3D viewer plugin-. The paracellular location of the
916 trypomastigote is shown. Green: CFSE-parasites. Red: LifeAct-RFP of HeLa
917 cells.

918

919 **S5 movie.**

920 The video shows the scanning of the first 20-30 μm (from the surface to the

921 center) of a CL Brener-infected spheroid after 1 h of incubation. Z-stack images
922 were obtained by confocal microscopy using 60x objective. The video was
923 realized by using ImageJ software. White arrow shows the paracellular located
924 trypomastigote. Green: CFSE-trypomastigotes. Gray: HeLa cells.

925

926 **S6 movie**

927 3D reconstruction of a single intracellular CL Brener trypomastigote located
928 inside the spheroid (20-30 μ m deep) after 1 h of incubation. Z-stack images were
929 obtained by confocal microscopy using 60x objective. The video was realized by
930 using ImageJ software -3D viewer plugin-. Green: CFSE-trypomastigotes. Red:
931 LifeAct-RFP of HeLa cells.

932

933 **S7 and S8 movies**

934 3D reconstruction of a HeLaR2 spheroid infected with CFSE-Y trypomastigotes
935 (video 7) or CFSE-RA trypomastigotes (video 8). Z-stack images were obtained
936 by confocal microscopy using 10x objective. The video was realized by using
937 ImageJ software -3D viewer plugin-. A half of an infected spheroids rotating on
938 the Y axis shown. Green: CFSE-parasites. Red: LifeAct-RFP of HeLa cells.

939

940

941

942

943

944

945

946

947

948

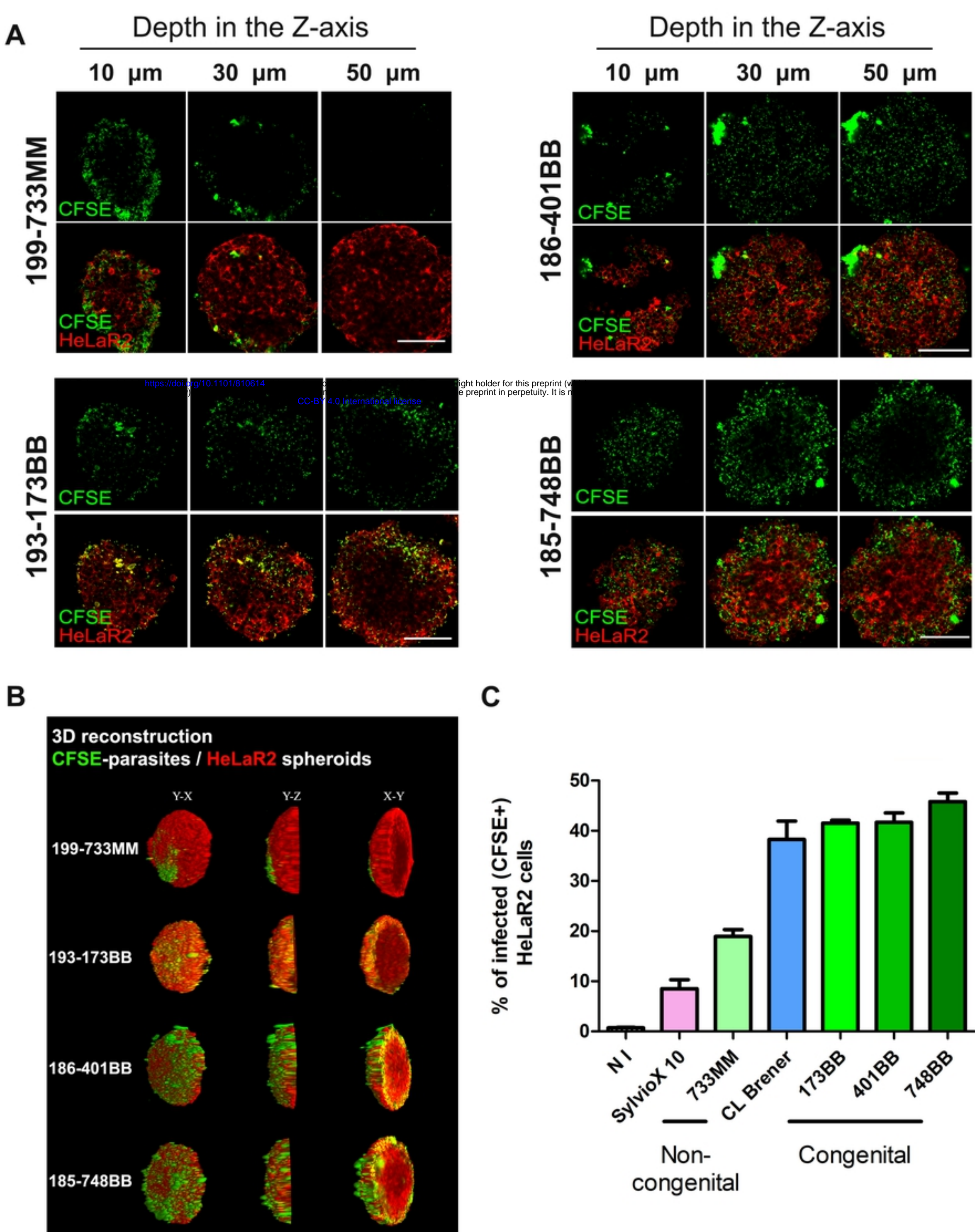


Fig 7

Depth in the Z-axis

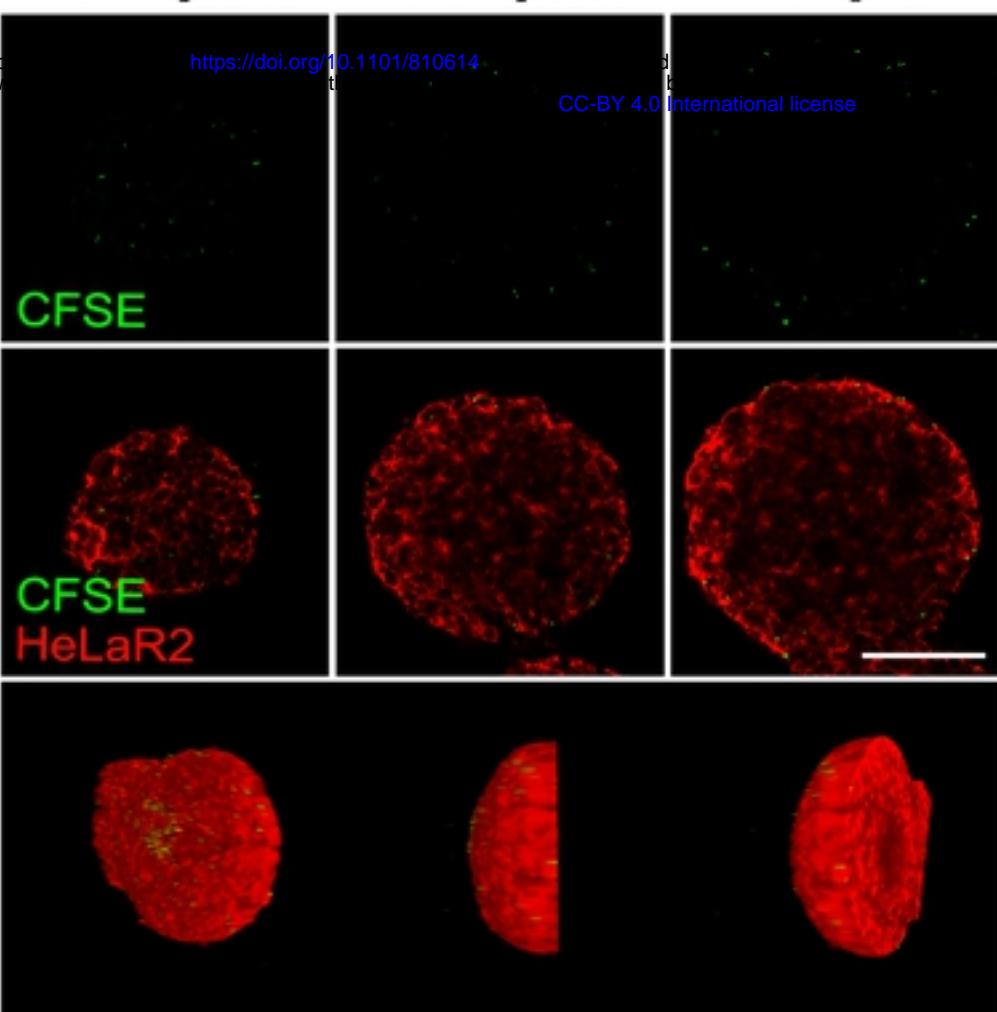
10 μm 30 μm 50 μm

<https://doi.org/10.1101/810614>

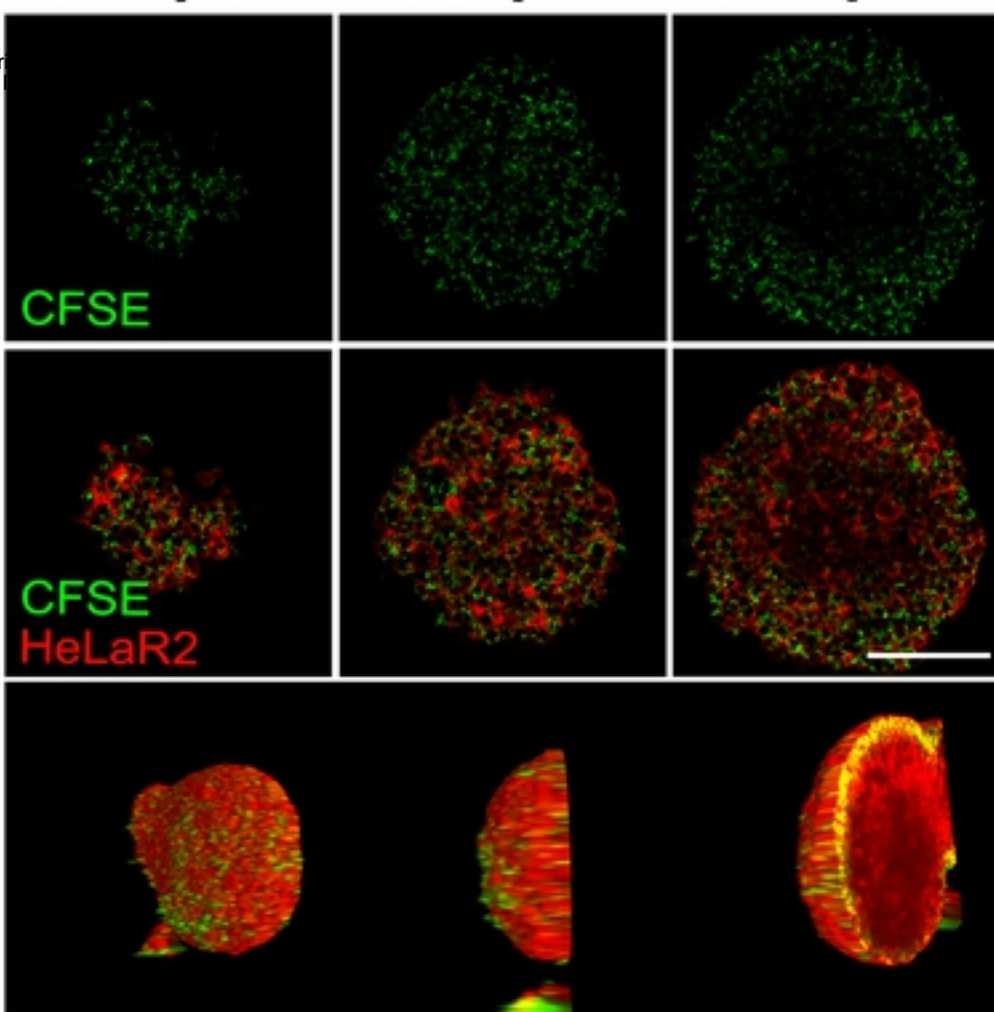
CC-BY 4.0 International license.

older for this preprint in perpetuity.

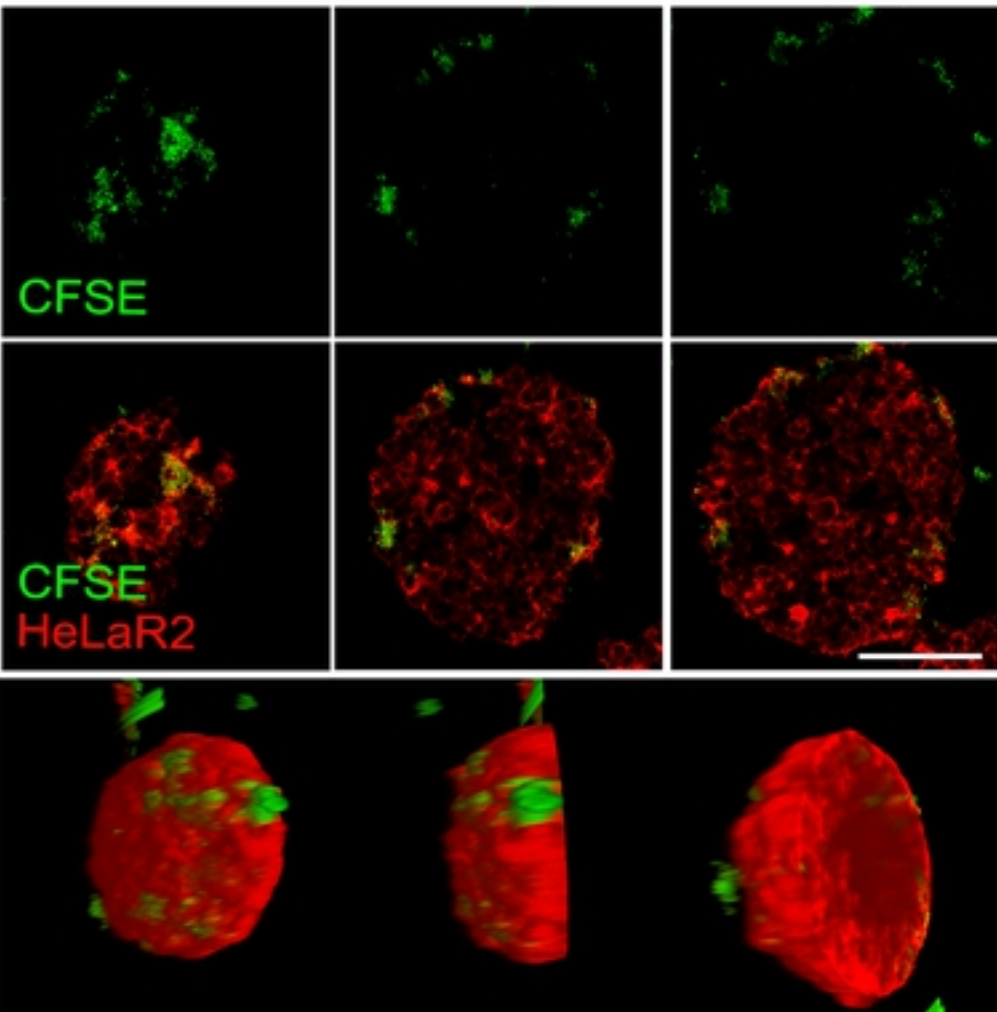
K98



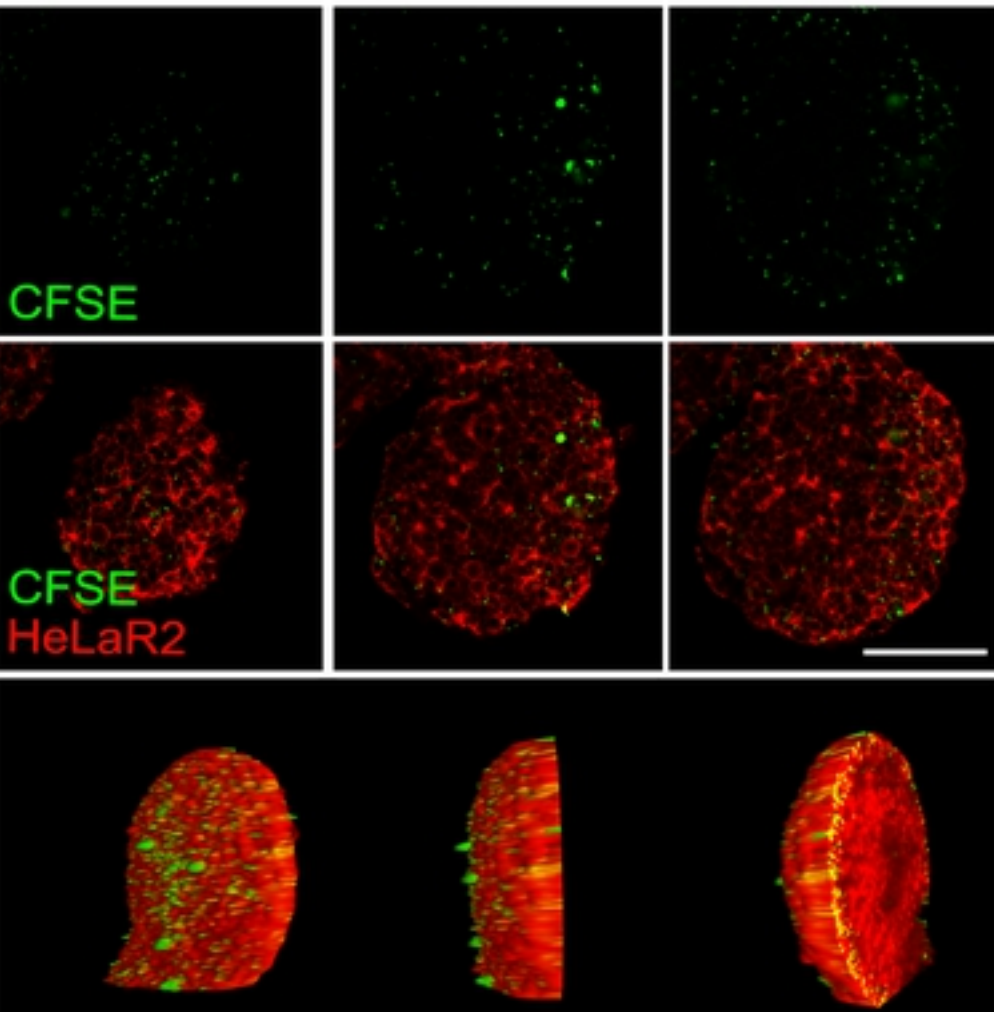
RA



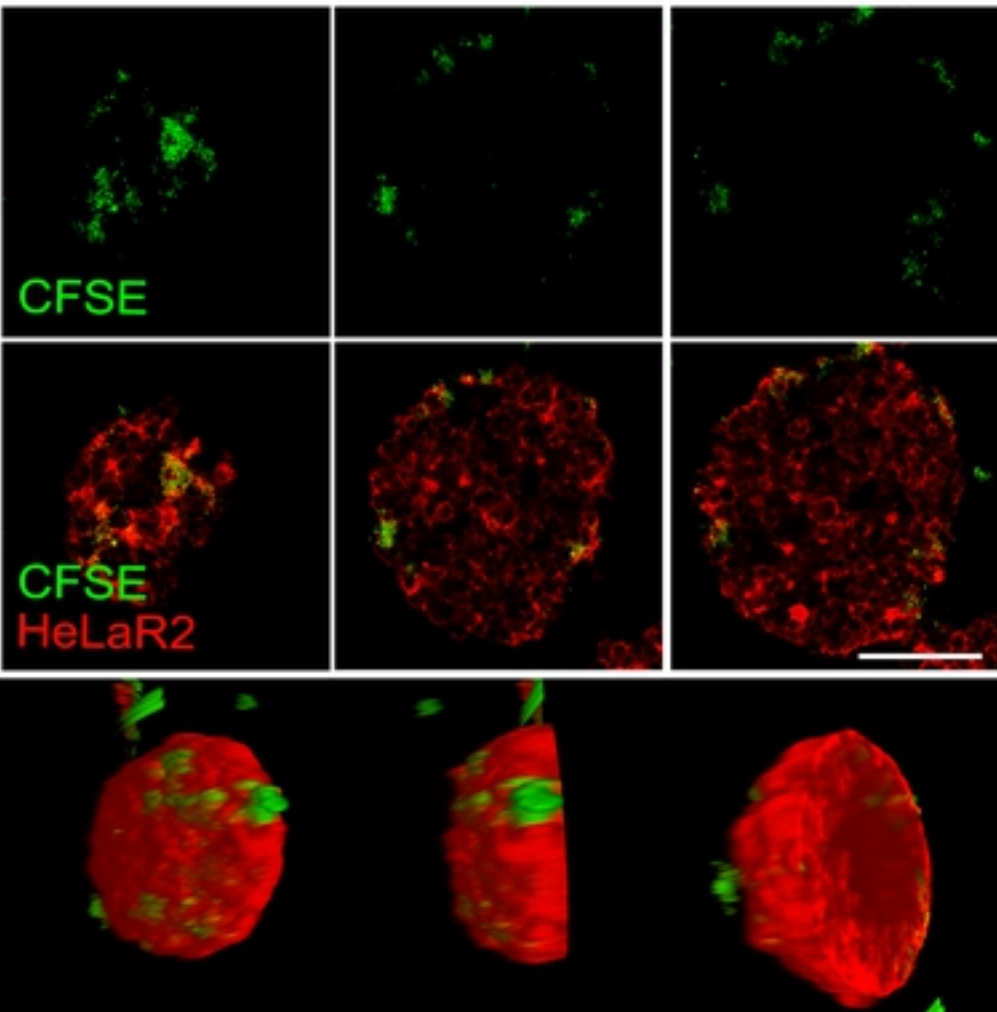
3D



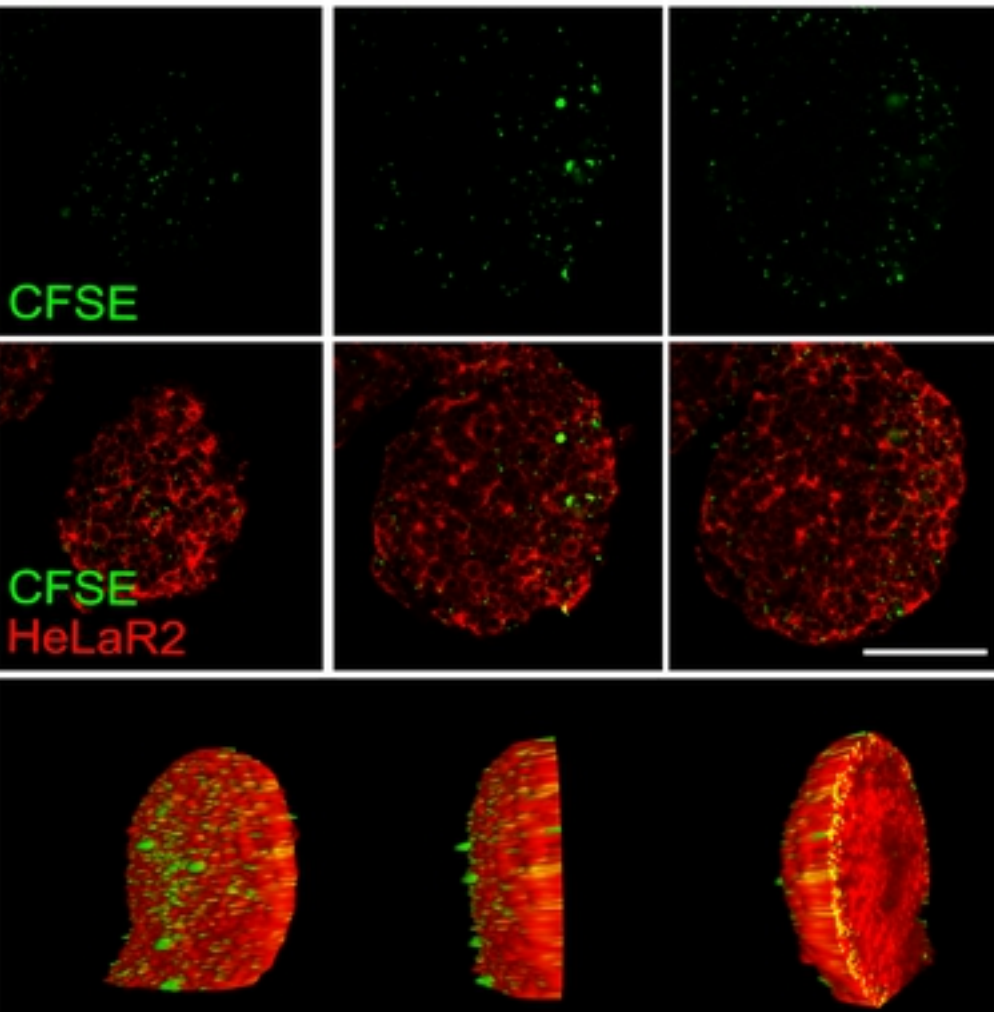
3D



Dm28c



Y



3D

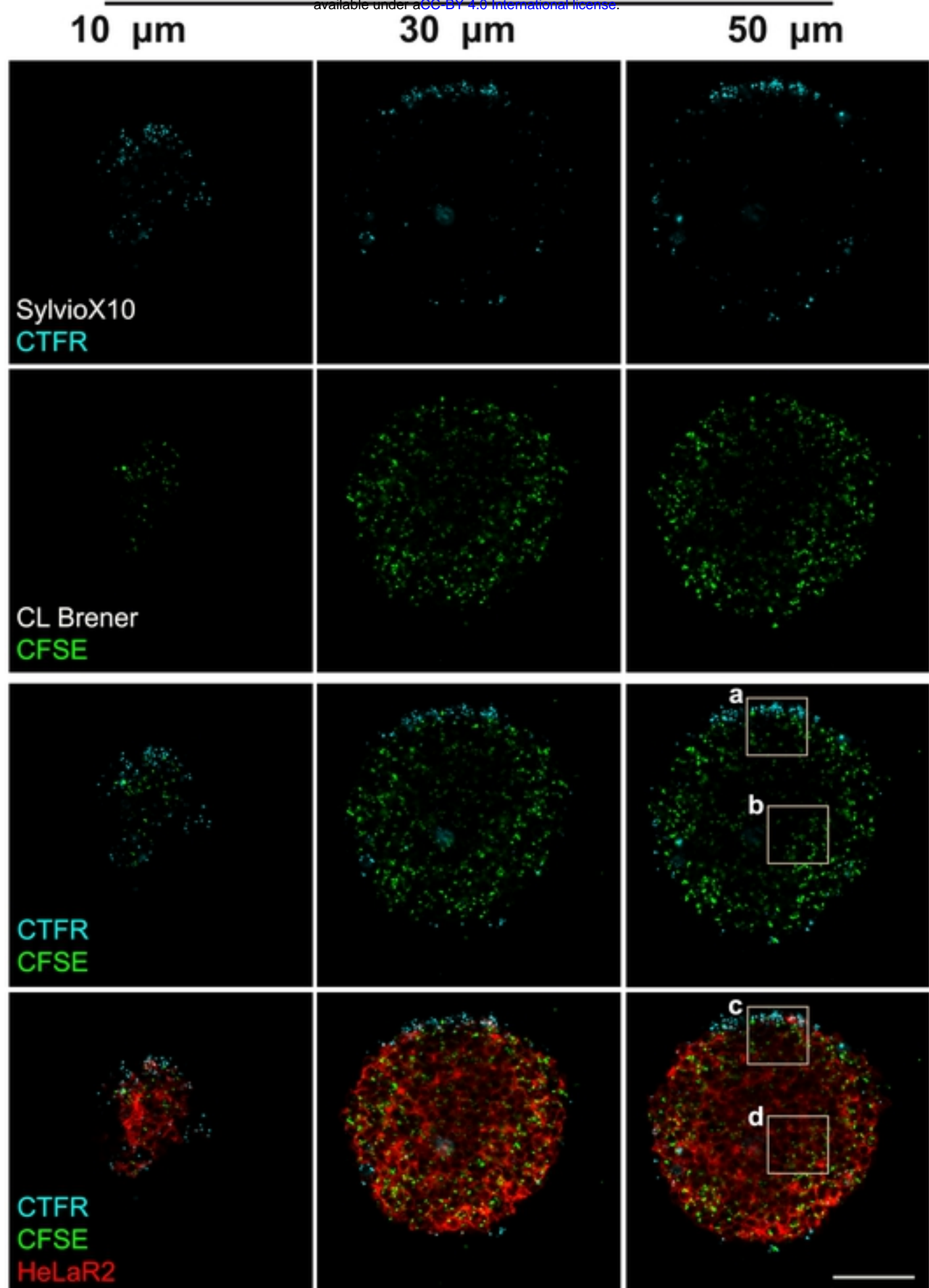
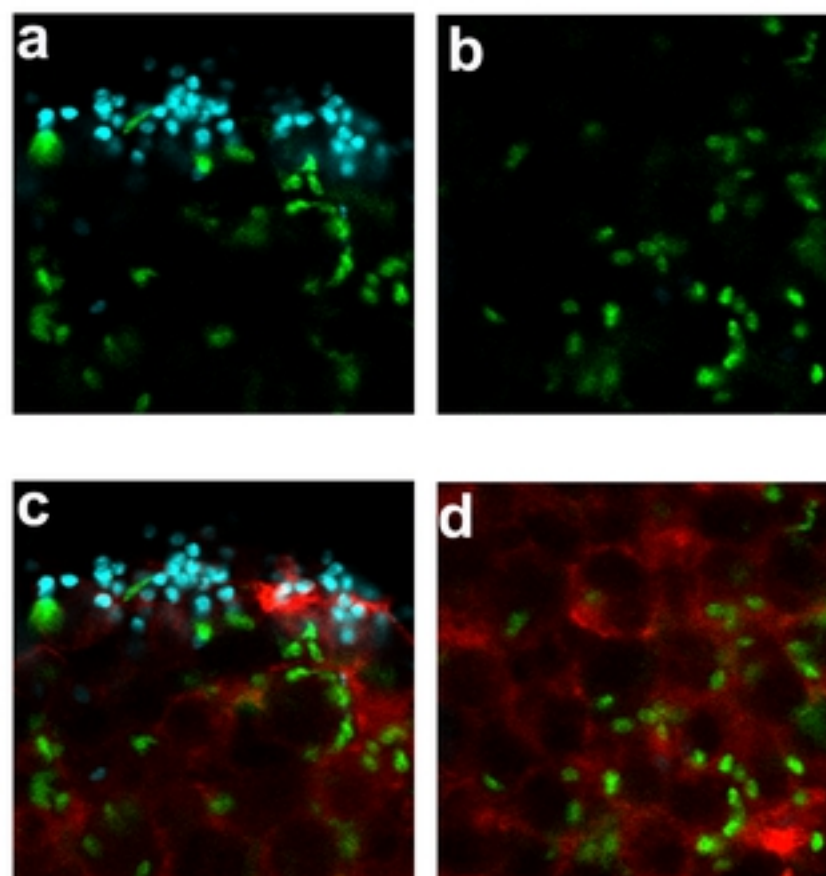
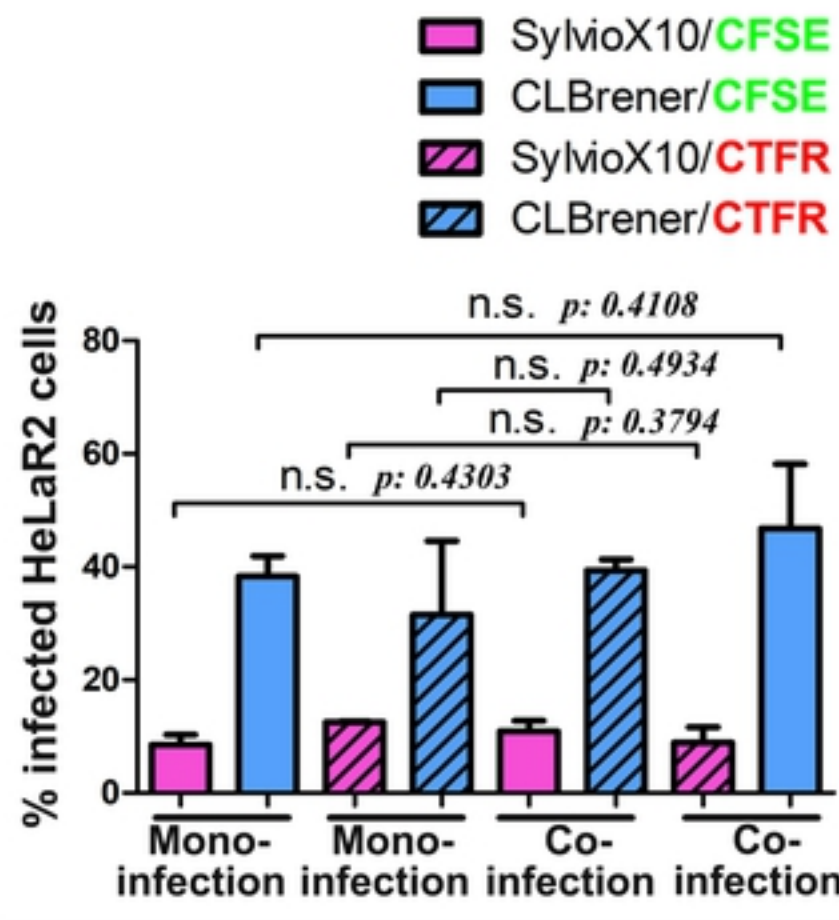
3D

Fig 6

A

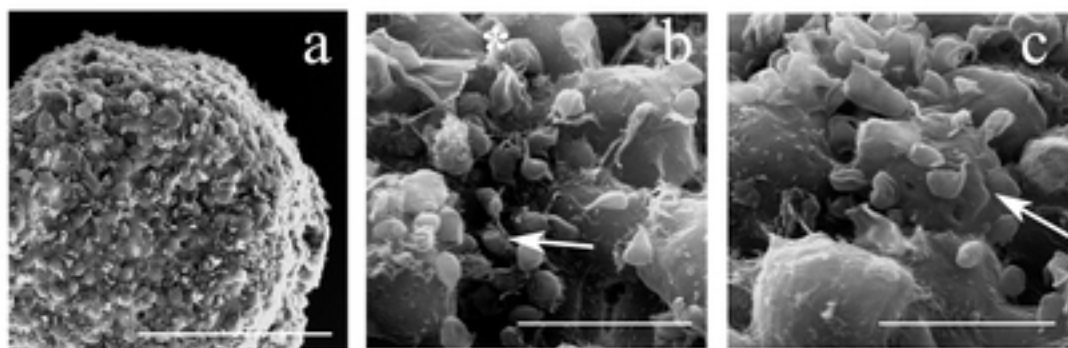
Depth in the Z-axis

bioRxiv preprint doi: <https://doi.org/10.1101/810614>; this version posted October 21, 2019. The copyright holder for this preprint (which was not certified by peer review) is the author/funder, who has granted bioRxiv a license to display the preprint in perpetuity. It is made available under aCC-BY 4.0 International license.

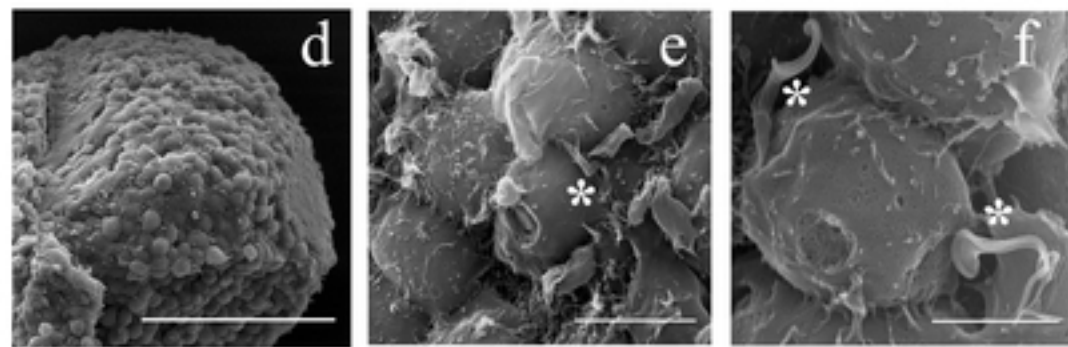
**B****Fig 5**

A

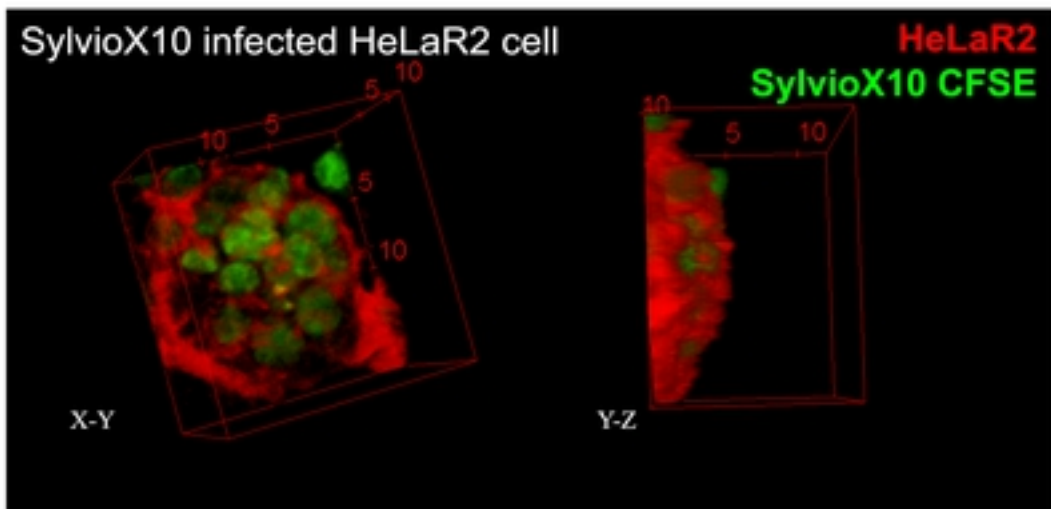
SylvioX10



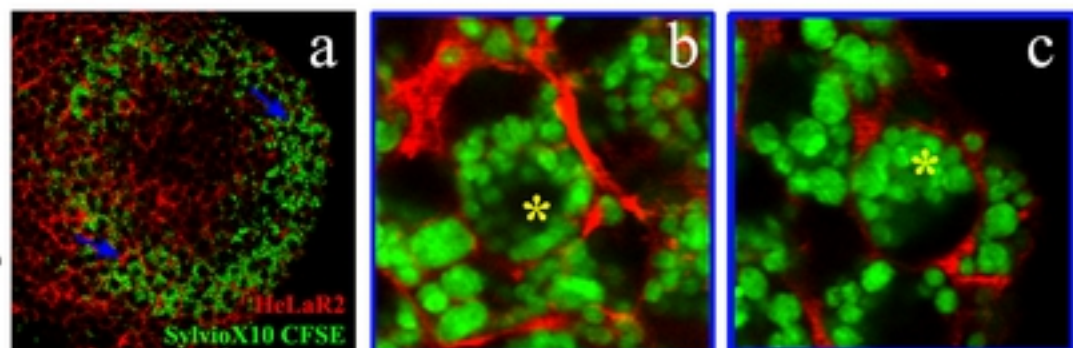
CL Brenr

**C**

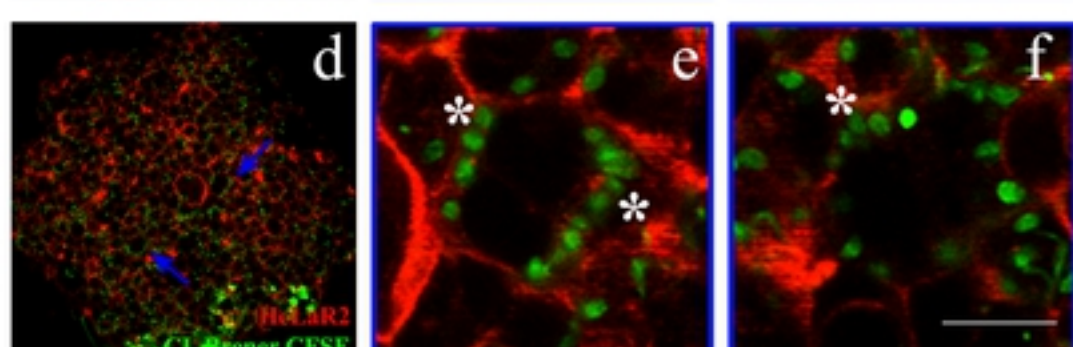
SylvioX10 infected HeLaR2 cell

**B**

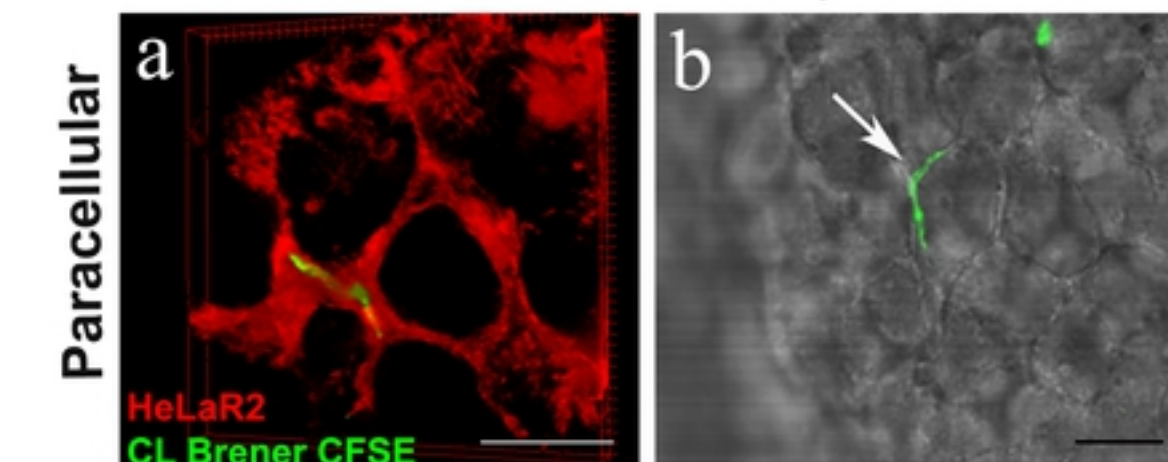
SylvioX10



CL Brenr

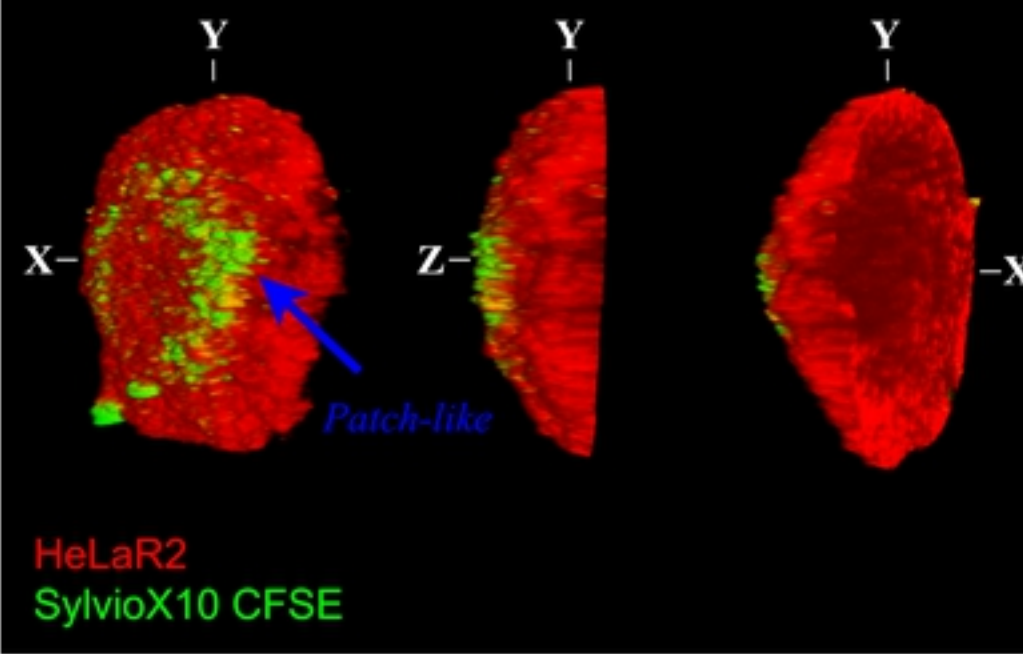
**Insets****D**

CL Brener infected spheroids

**Fig 4**

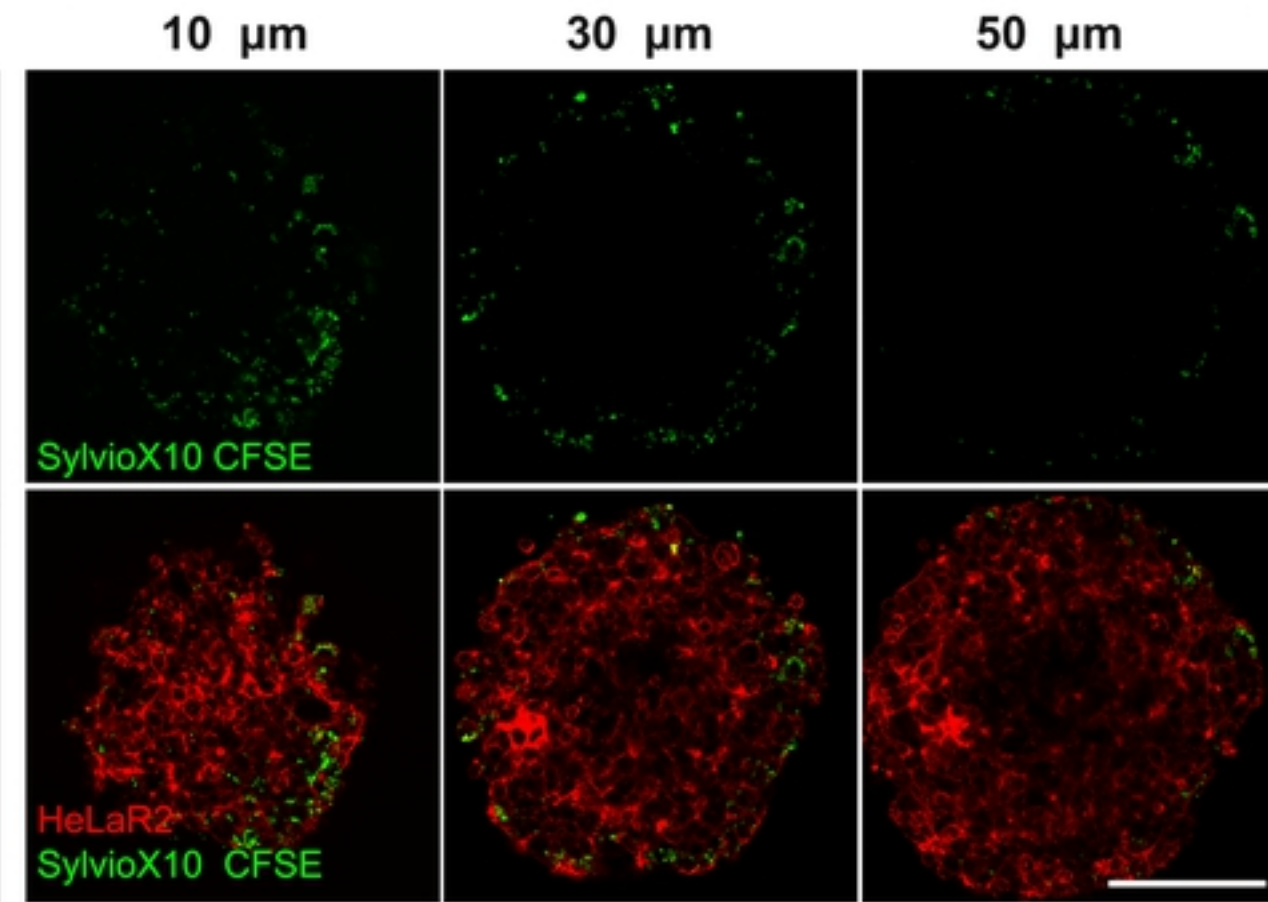
A

3D reconstruction



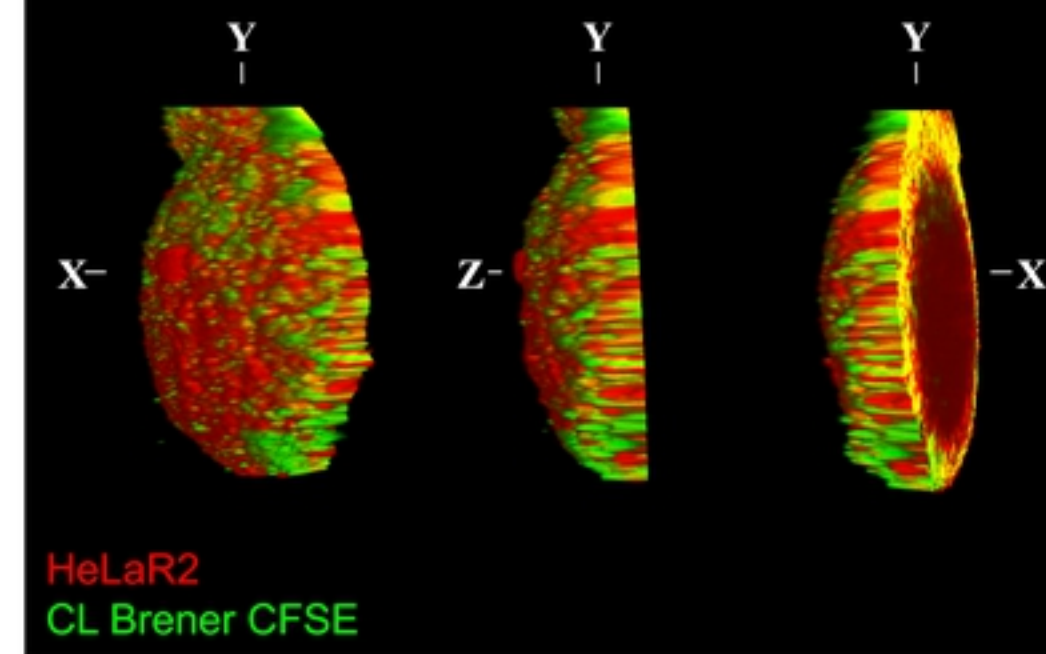
C

Depth in the Z-axis



B

3D reconstruction



D

Depth in the Z-axis

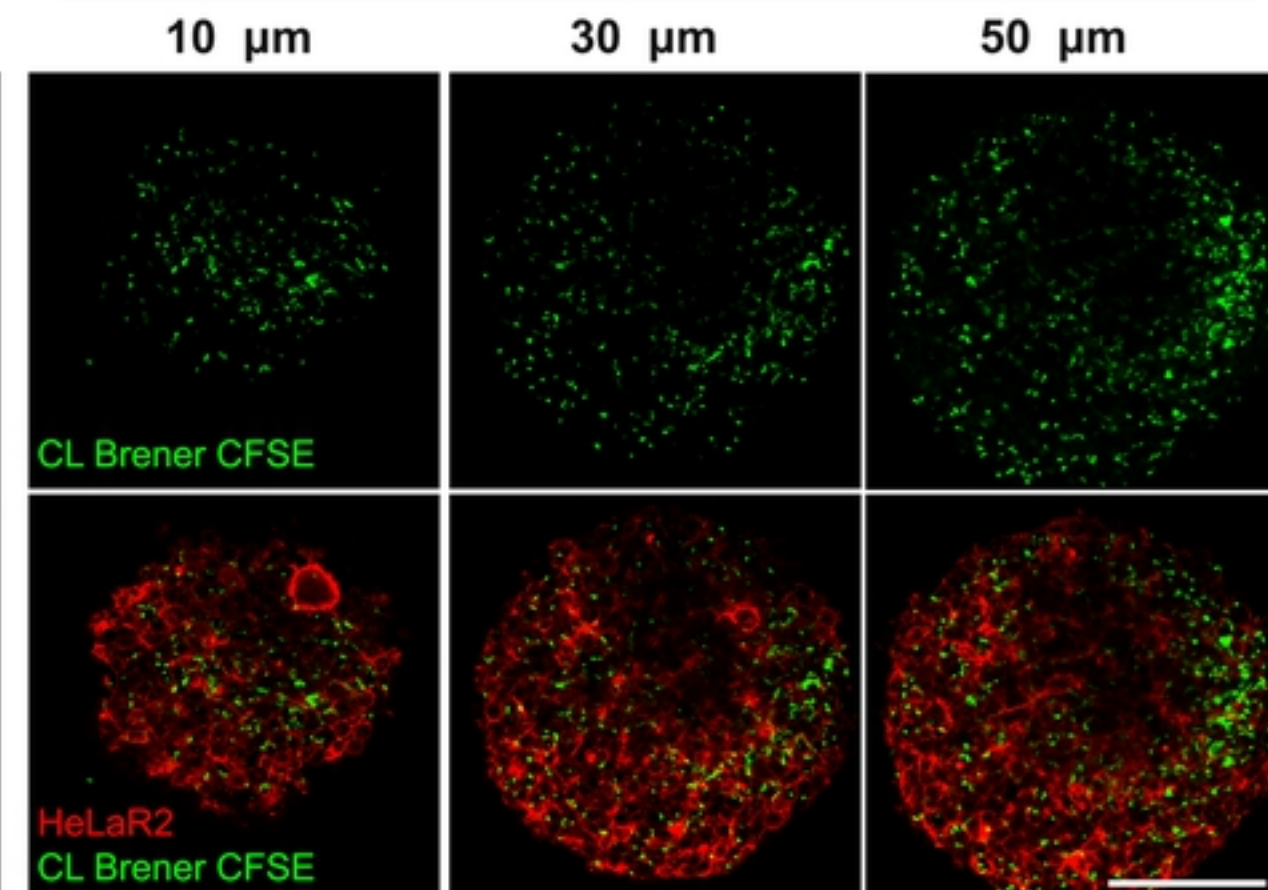
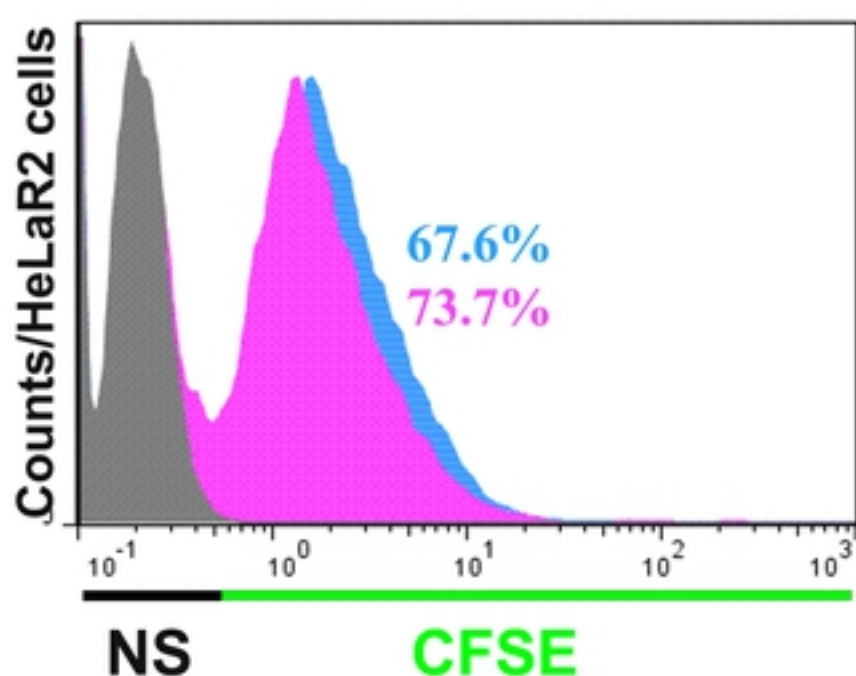


Fig 3

■ Non-infected ■ SylvioX10 ■ CL Brener

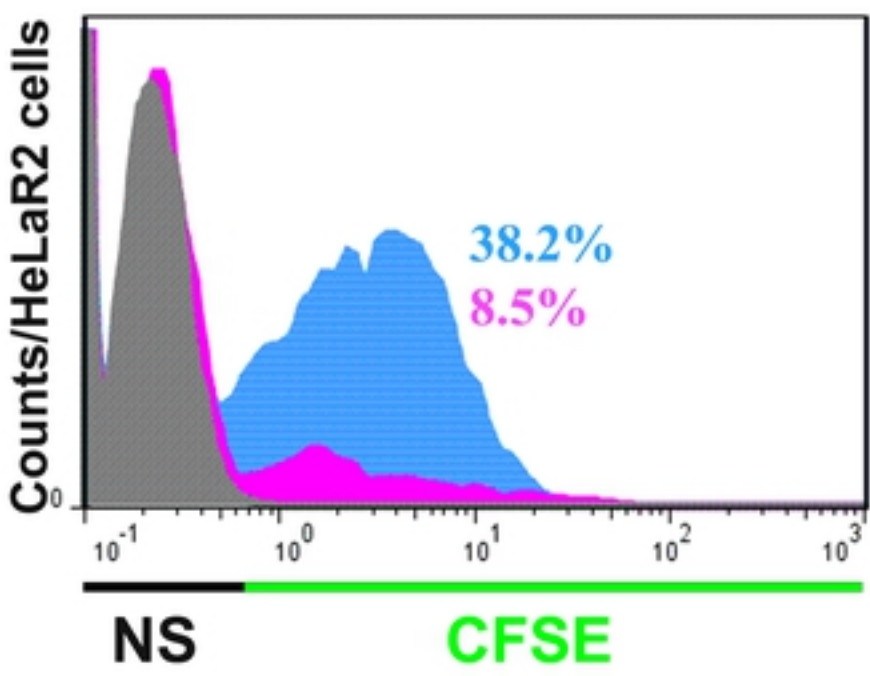
A

2D-monolayer



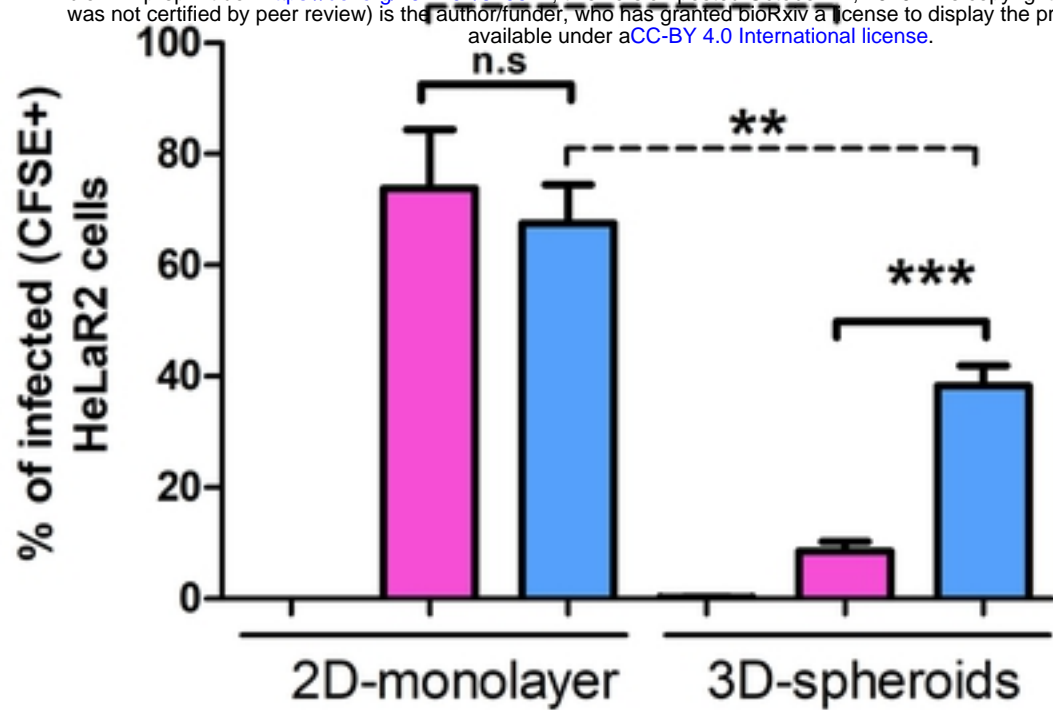
B

3D-spheroids

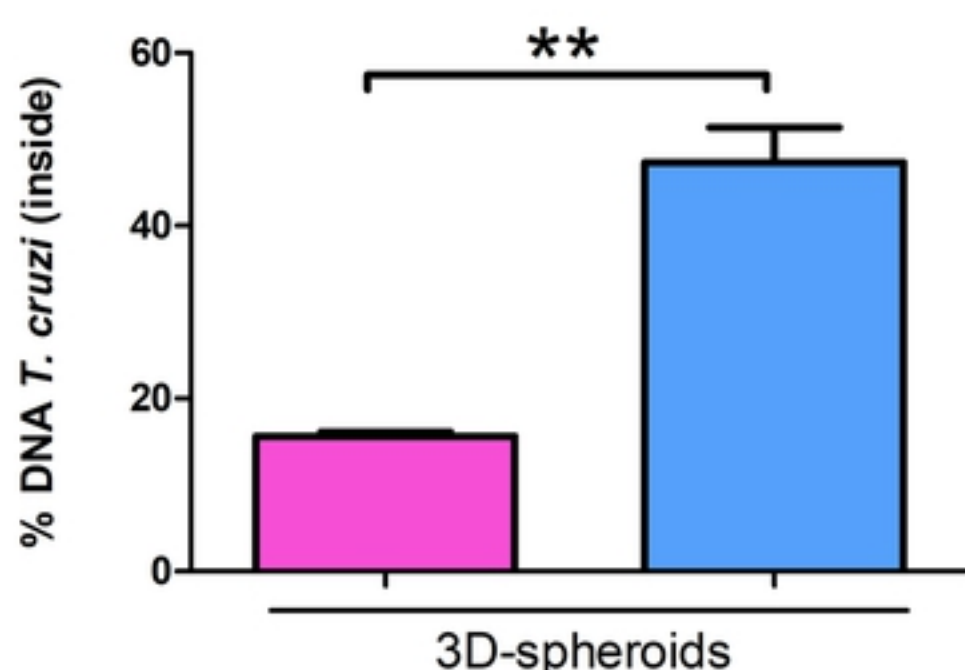


C

bioRxiv preprint doi: <https://doi.org/10.1101/810614>; this version posted October 21, 2019. The copyright holder for this preprint (which was not certified by peer review) is the author/funder, who has granted bioRxiv a license to display the preprint in perpetuity. It is made available under aCC-BY 4.0 International license.



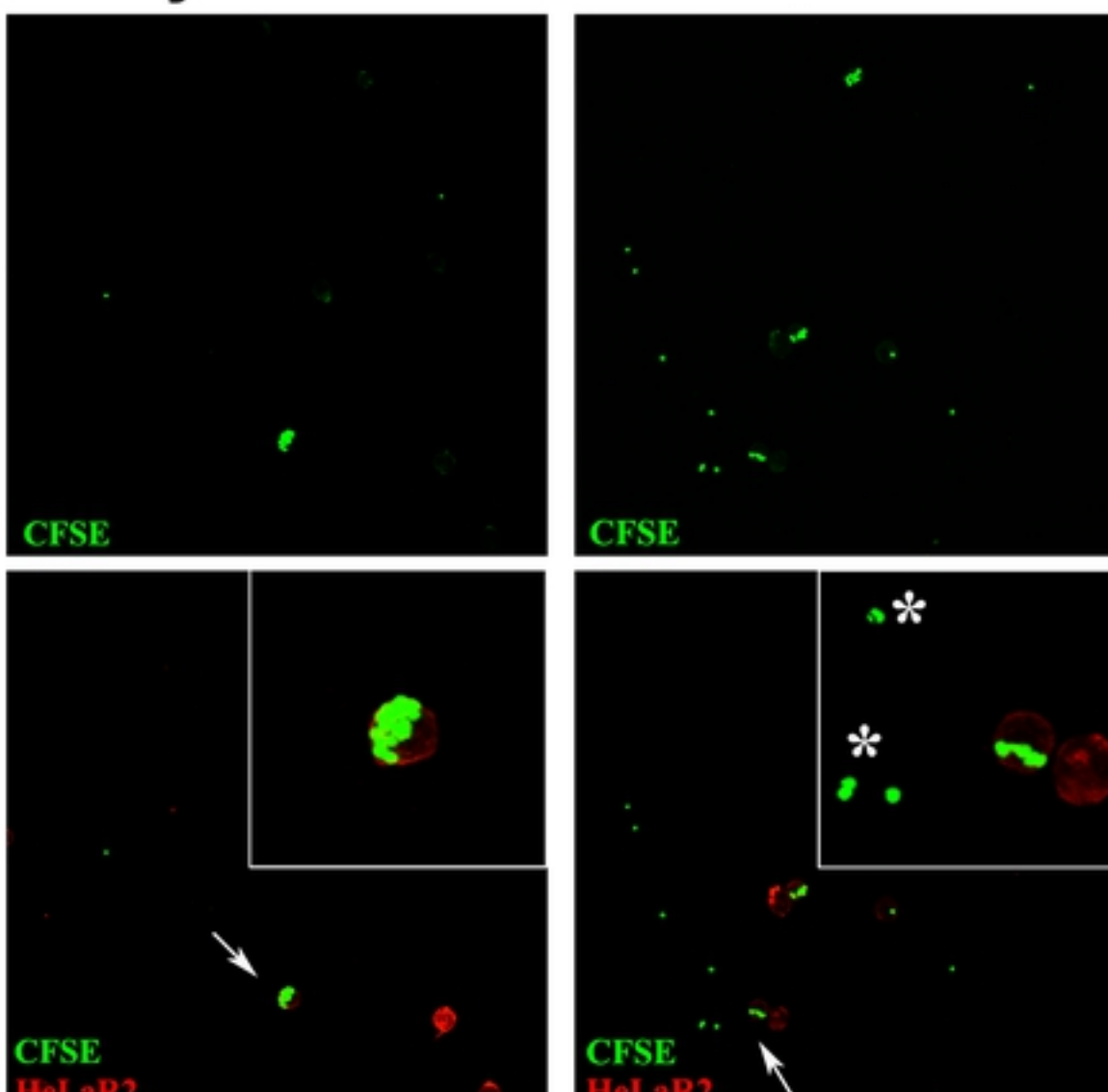
D



E

SylvioX10

CL Brener



F

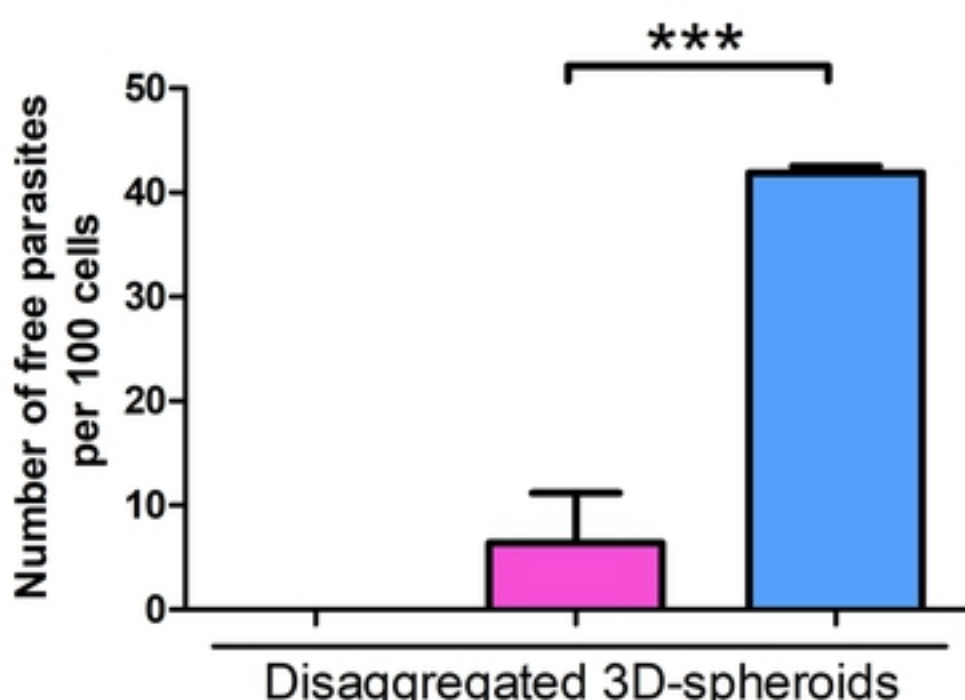
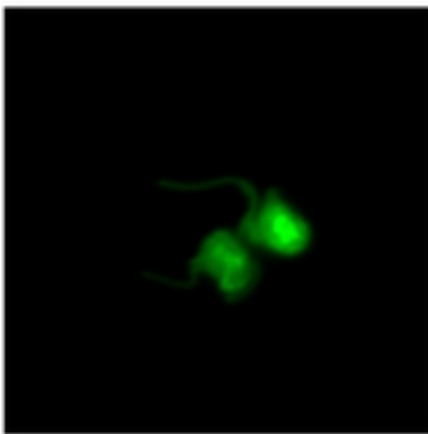
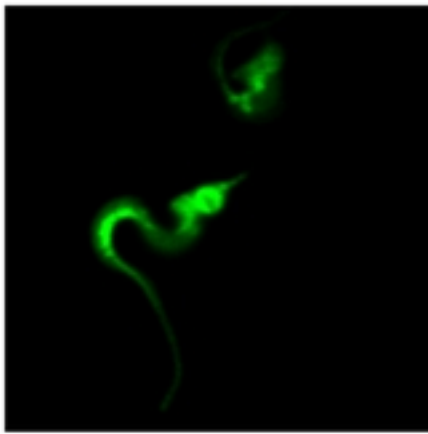


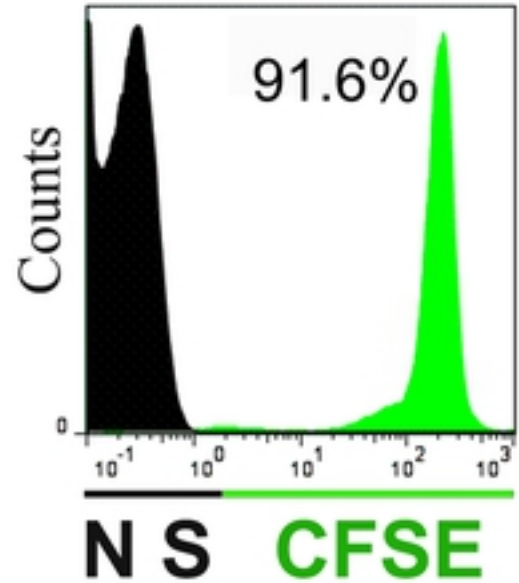
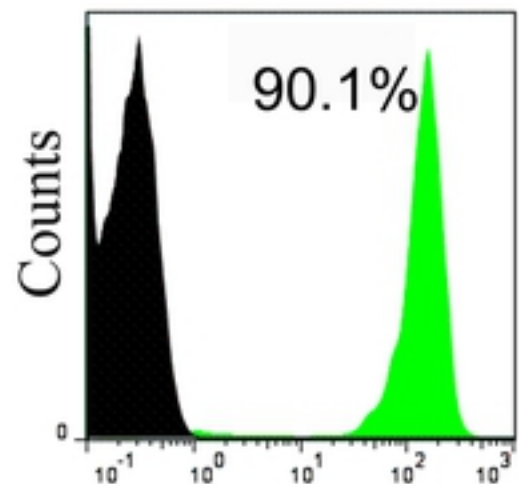
Fig 2

A

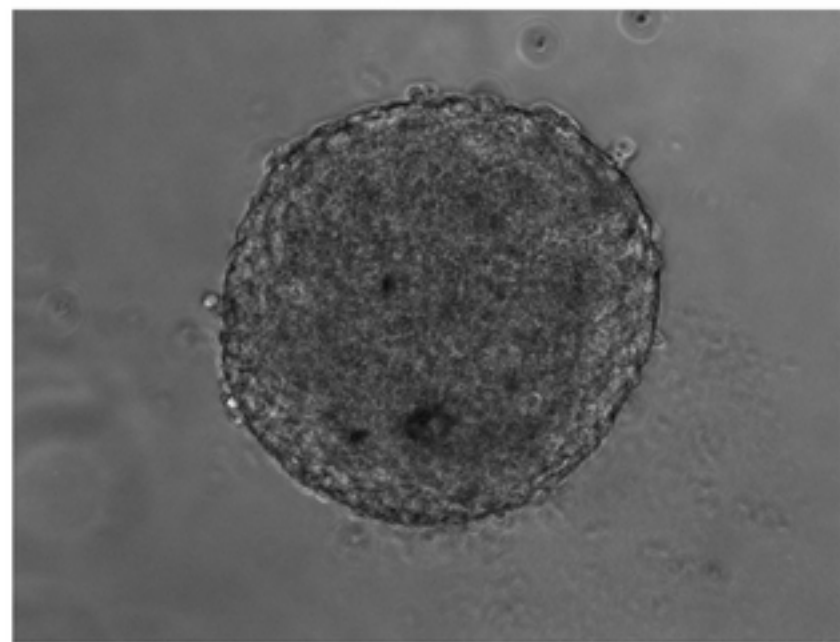
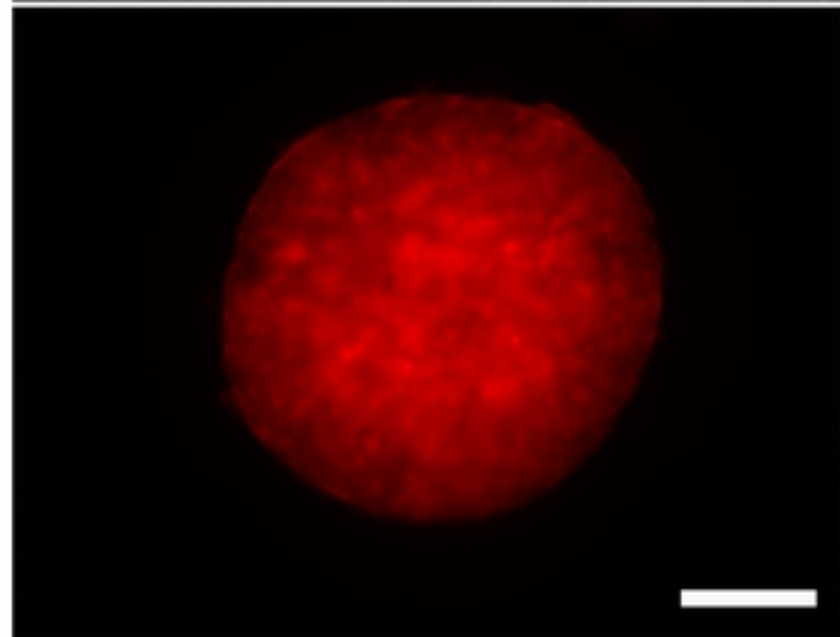
Microscopy

SylvioX10**CL Brener****CFSE**

Flow cytometry

**B**

3D Spheroid

Bright**LifeAct-RFP****Fig 1**